ERDC/CRREL TR-11-8

Cold Regions Research and Engineering Laboratory

US Army Corps of Engineers®
Engineer Research and Development Center

Assessing the Accuracy of Passive Microwave Estimates of Snow Water Equivalent in Data-Scarce Regions for Use in Water Resource Applications

A case study in the Upper Helmand Watershed, Afghanistan

Carrie M. Vuyovich

March 2011

ERDC/CRREL TR-11-8
March 2011

Assessing the Accuracy of Passive Microwave Estimates of Snow Water Equivalent in Data-Scarce Regions for Use in Water Resource Applications

A case study in the Upper Helmand Watershed, Afghanistan

Carrie M. Vuyovich

Cold Regions Research and Engineering Laboratory
U.S. Army Engineer Research and Development Center
72 Lyme Road
Hanover, NH 03755

Final report

Prepared for U.S. Army Corps of Engineers
Washington, DC 20314-1000

Abstract: Winter snowpack is a significant contributor to water supply in many regions of the world and accurate estimates of the snow water equivalent (SWE) are necessary for water resource planning. Satellite data are an attractive source of snow information in remote regions with limited ground data. The objective of this study is to assess passive microwave SWE in the Upper Helmand Watershed in Afghanistan where snowmelt is a primary source of water. Passive microwave SWE data were compared over six winter seasons, 2004–2009, to an independent estimate of SWE using a snow hydrology model. The snow hydrology model was calibrated to high-resolution snow covered area images and observed reservoir levels. The model was initialized with passive microwave SWE data and found to improve results in years when input precipitation was low. The results showed that passive microwave SWE has potential to provide valuable water resource information in this data-scarce region.

Table of Contents

List of Figures and Tables

Figures

Tables

Preface

This report was prepared by Carrie M. Vuyovich, Research Hydraulic Engineer, Remote Sensing/GIS and Water Resources Branch (RR-CI), U.S. Army Engineer Research and Development Center (ERDC), Cold Regions Research and Engineering Laboratory (CRREL), Hanover, New Hampshire.

Funding for this project was provided by USACE Headquarters and ERDC-CRREL Long Term Training program to support a Masters Degree in Civil Engineering at the University of New Hampshire.

This report was prepared under the general supervision of Timothy Pangburn, Branch Chief, RS/GIS and Water Resources Branch, CRREL; Dr. Justin B. Berman, Chief, Research and Engineering Division, CRREL; Dr. Lance D. Hansen, Deputy Director, CRREL; and Dr. Robert E. Davis Director, CRREL. The Commander and Executive Director of the ERDC is COL Kevin J. Wilson. The Director is Dr. Jeffrey P. Holland.

1 Introduction

Snowmelt is a primary source of water in many mountainous regions of the world. Runoff from snowmelt has far-reaching impacts to areas where snow never falls but that rely upon melt water to fill streams and reservoirs and replenish aquifers. To meet various water demands, including agriculture, drinking water, flood control and navigation, to plan for future demands, and to assess the condition of water resources, an accurate assessment of the volume of water contained in the snowpack is necessary. An estimated 15% of the world's population lives in regions that depend heavily on snowmelt for water supply (Barnett et al. 2005; UNESCO 2009). With populations and, therefore, water demand expected to rise in the near future (Cosgrove and Rijsberman 2000), all sources of water will become increasingly valuable and must be assessed to make sure these demands can be met.

Several methods and technologies are used for measuring the snowpack (DeWalle and Rango 2008). Ground measurements are taken by using gages such as snow pillows, snowboards, and rain gages. Manual measurements are made at point locations or over a length by snow surveys. Remote sensing technologies are also employed to measure snow, using methods such as gamma radiation, active and passive microwave radiation, and visible imagery. Often, several methods are employed to arrive at the best estimate of the volume of water contained in the snow and to minimize error associated with any individual method.

Numerical models are also used to estimate the snowpack based on meteorological data and ground conditions. The two most widely used approaches to modeling snow are a complete energy balance method and a temperature index method The energy balance method calculates snowmelt by estimating the incoming and outgoing energy fluxes; several implementations of this method have been developed (Jordan 1991; Marks et al. 1999; Frankenstein et al. 2008). This method accurately represents the heat transfer process within the snowpack. However, the significant data requirements of an energy balance model can make it difficult to use in an operational setting.

The temperature index method calculates melt using the difference between air temperature and snowpack temperature as a surrogate for the net incoming energy. A linear relationship is assumed between this temperature difference and the snowmelt rate. This is a reasonable assumption as the air temperature is physically associated with the predominant energy fluxes associated with melt (Ohmura 2001). This is particularly true in forested areas; however, in open regions, shortwave radiation and wind can also play significant roles and this method may not work as well (USACE 1998). Temperature index models have been widely used in hydrologic applications because of the availability of temperature data, and because model results generally provide reasonable estimates of stream flow (Hock 2003; Franz et al. 2008).

All techniques for measuring and modeling snow have error and in some cases the error can be significant. Rain gage measurements are susceptible to wind undercatch and equipment error. In addition, point measurements introduce error when distributed over a large heterogeneous area. Remote sensing relies on assumptions about the snowpack, which may change from place to place or over the course of the winter. Numerical models are only as good as the data used to drive them. Regardless, accurate, unbiased estimates of the snowpack are needed to improve the efficiency of water use and to provide valuable information during extreme years.

In developing countries and very remote regions, assessing the volume of water contained in the snowpack can be especially difficult. Snow data are rarely available. Financial constraints or safety concerns, or both, may limit the instrumentation and personnel that are deployed to take measurements. Without information about the snowpack, these regions are especially susceptible to flooding or drought. In addition, inefficient water management can add to the economic hardship of the population. Remote sensing is an attractive method to obtain information about the snowpack when other data sources are limited.

The two main types of snow data derived from satellites are snow covered area (SCA) and snow water equivalent (SWE). SCA can be detected at high-resolution using optical sensors. Snow contrasts greatly with its surroundings owing to its high albedo and can be easily detected. Satellite estimates of SCA have been found to be highly accurate (Gafurov and Bardossy 2009). SCA images cannot be taken at night or through a cloud cover, and no information is derived about snow depth or water volume

contained in the snowpack. Still, it has been successfully used in hydrologic applications. The snow runoff model (SRM) uses SCA and a basin-specific snow depletion curve to model snowmelt (Martinec et al. 2008). Many studies have successfully modeled snow runoff using SRM (Li and Williams 2008; Immerzeel et al. 2009). Other studies have used SCA for data assimilation to improve model accuracy (Andreadis and Lettenmaier 2006; Nagler et al. 2008).

SWE, the volume of water contained in the snowpack, can be estimated remotely by measuring the passive microwave signal naturally emitted from the Earth. A passive microwave signal at wavelengths greater than 25 GHz is scattered as it passes through the snowpack. An estimate of the SWE is obtained by taking the difference between the return signal at two different passive microwave wavelengths: a low wavelength that is not scattered by the snow, at approximately 19 GHz, and a high wavelength that is, typically, around 37 GHz. The calculated SWE is proportional to the difference. Passive microwave sensors make two daily passes around the globe and can provide data during cloud cover and at night.

Equations to estimate SWE typically follow a formulation:

$$SWE = c(Tb_{19} - Tb_{37}) \tag{1}$$

where

SWE = snow water equivalent (mm)
Tb_{37} = return signal, or brightness temperature (37 GHz)
Tb_{19} = brightness temperature at 19 GHz
c = radiative transfer coefficient (Foster et al. 2005)

Coefficients have been developed empirically, using data from specific regions, thus revising the coefficient for a particular area may improve results (Rawlins et al. 2007).

SWE data are particularly important for hydrologic applications because the volume of water available is a primary concern. However, the accuracy of passive microwave SWE estimates has limited its use in water resource applications. Passive microwave signals are affected by the natural conditioning of the snowpack and the geography of the land. Wet snow can reduce the signal (Hallikainen et al. 1986; Walker and Goodison 1993). Large snow crystals, or depth hoar, caused by very cold, dry conditions can

increase the signal (Hall et al. 1986; Foster et al. 1999; Josberger and Mognard 2002). Topology of the ground (Matzler and Standley 2000) and vegetation (Derksen et al. 2003, 2005) have also been shown to affect the passive microwave estimate of SWE.

Currently, the satellite-based estimates of SWE are not accurate enough to replace ground-based measurements in regions with a sufficient network of gages, though as technology and accuracy improve, the applications of remotely sensed SWE will almost certainly increase. The main goal of this study aims to determine if remotely sensed SWE provides value or enhances the skill of specific water resource applications in remote regions without sufficient ground measurements. For instance, can passive microwave data be used to predict the relative magnitude of spring runoff so as to make reservoir regulation decisions? In a region with limited data, assessing the accuracy of satellite data is difficult but necessary to provide confidence to the estimates.

This study will compare passive microwave estimates of SWE in a remote, mountainous watershed in Afghanistan to results of a snow hydrology model of the same region. The model is validated by comparing simulated runoff to reservoir measurements at the basin outlet. Chapter 2 provides an overview of the study location, the available data, and the method of analysis. In Chapter 3 the results are presented in three areas: preliminary analyses of the data quality, snow model results, and hydrologic model results. The results are discussed in Chapter 4, and Chapter 5 gives final conclusions.

2 Methods

2.1 Site Description

The study region is the Upper Helmand watershed in central Afghanistan. The watershed is approximately 47,000 km^2 and extends from the Hindu Kush Mountains in the northeast to the Kajakai Reservoir in the southwest (Fig. 2-1). Elevations range from 4085 m at the divide to 1000 m at the dam. The Helmand River, the longest river in Afghanistan, originates in the Upper Helmand watershed and flows approximately 500 km to the Kajakai Reservoir, and then another 610 km until it reaches the Sistan Delta on the border with Iran. The Helmand River is a main source of water for the southern region of Afghanistan.

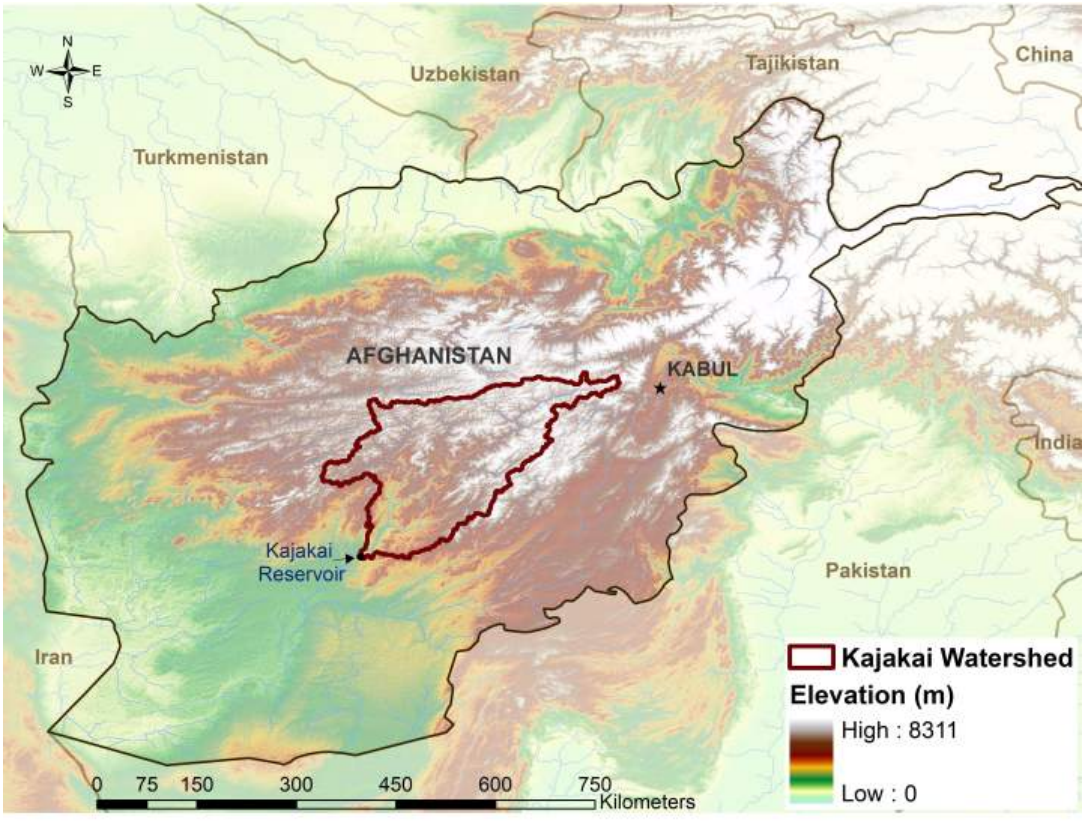

Figure 2-1. Site of Upper Helmand watershed in central Afghanistan.

Snowmelt contributes a significant portion of the total runoff to the Helmand River. According to the Watershed Atlas of Afghanistan (Favre and Kamal 2004), 80% of Afghanistan's water resources come in the form of snow. Snowmelt and increased rainfall in the spring provide water neces-

sary to sustain crops and irrigation. By late summer, streamflows decrease significantly. Precipitation in Afghanistan is consistent with a sub-arid climate. Climatology data show an average annual precipitation of 200–400 mm over central Afghanistan (NCDC 2010). Figure 2-2 shows the typical annual cycle of streamflow, precipitation, and temperature based on historical data in central Afghanistan.

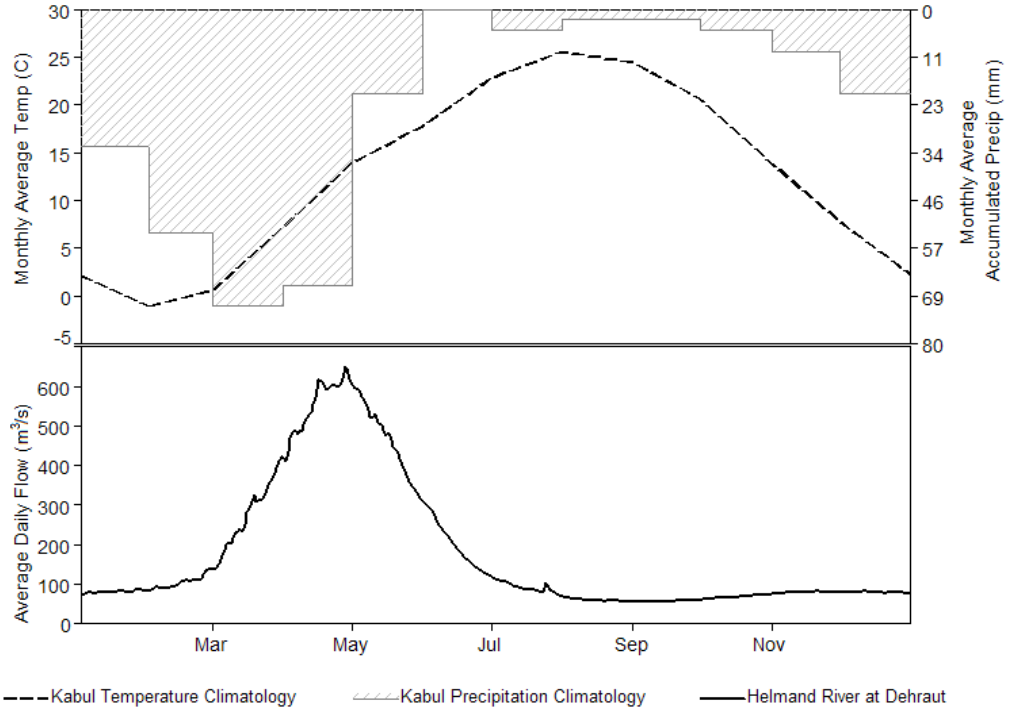

Figure 2-2. Historical stream flow and climatology data.

The Kajakai Reservoir was formed when a dam was built in 1953 (Fig. 2-3). The dam regulates the Helmand River for irrigation and flood control. In 1975, a powerhouse was added to supply electricity to southern Afghanistan. This project is economically important to the region and future increases to capacity have been investigated (USACE 2007). Two 16.5-MW generating units are currently in operation with the potential for a third unit to be installed. The emergency spillway was never completed to the design elevation of 1045.0 m. It currently exists as an uncontrolled spillway with an approximate elevation of 1033.6 m.

Figure 2-3. Aerial view of Kajakai Dam (from www.afghaneic.org).

Several studies have investigated the hydrologic conditions of the Upper Helmand watershed to evaluate the design and operational capacity of the project. A 1976 hydrologic analysis of the basin (Harza 1976) estimated the probable maximum flood (PMF) for the design of the spillway gates. More recently, Burger (2005) modeled the entire Helmand basin to understand the Sistan Delta region. USACE (2007) analyzed the ability of the reservoir to meet demands based on a statistical analysis of historical data. USGS (2007) simulated future runoff conditions to assess the ability of the reservoir to meet demands under various operational and climate change scenarios. For this study the watershed was subdivided into 11 smaller basins to capture differences among regions within the larger watershed (Fig. 2-4). Basins having higher elevations receive a greater percentage of precipitation as snow and may exhibit different runoff patterns from the lower, warmer regions.

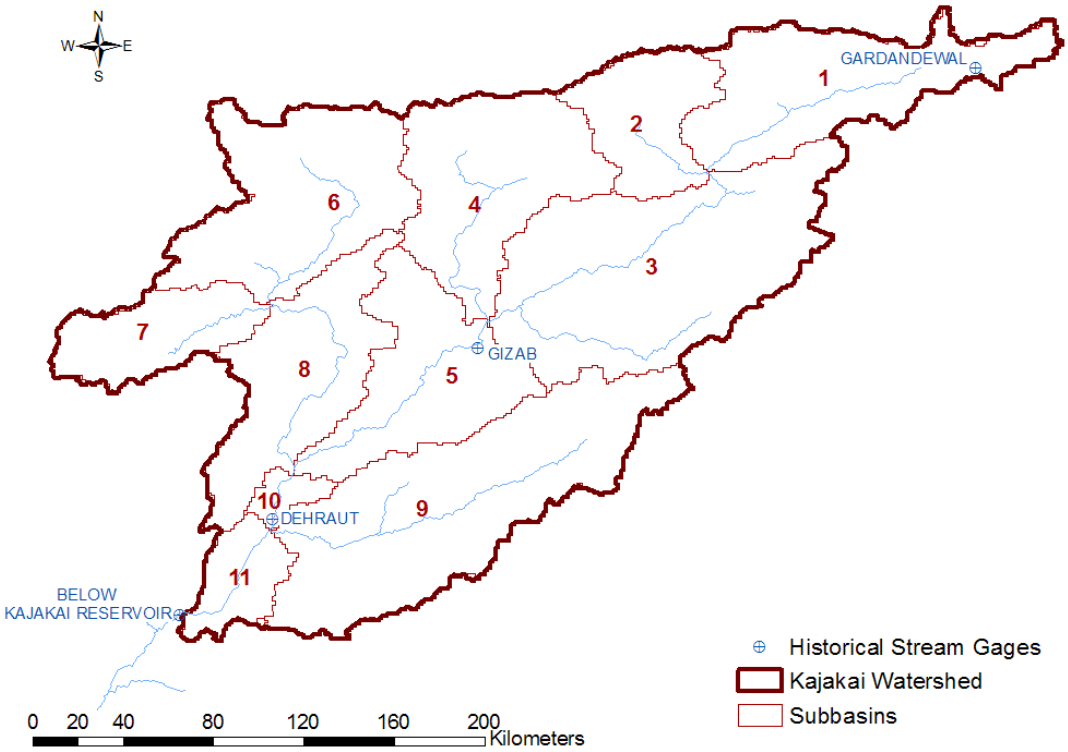

Figure 2-4. Upper Helmand watershed, subbasins, and historical stream gages.

2.2 Data

Ground data are scarce in all of Afghanistan, including the Upper Helmand Watershed. A system of stream gages along the Helmand River routinely recorded data beginning in the 1940s until being discontinued during the Soviet invasion in 1979 (Williams-Sether 2008). Meteorological data were limited and unreliable prior to 1980. Since 2003, a number of stations have been reestablished and are consistently recording. Data collection has been maintained at many of the dam and irrigation projects, though much of these data are stored locally and can be difficult to access. Snow data are particularly difficult to obtain given the rugged terrain and limited access. While snow data are available through remote sensing, no ground-based data are available specifically for Afghanistan. The following sections describe the data available and derived for use in this study; these are also summarized in Table 2-1.

Table 2-1. Available data for the Helmand Watershed, Afghan study site.

Data Type	Period of Record	Source
Historical Stream flow on Helmand River		
Helmand River at Dehraut	1952–1979	http://waterdata.usgs.gov
Helmand River at Gizab	1971–1979	http://waterdata.usgs.gov
Helmand River at Gardandewal	1969–1980	http://waterdata.usgs.gov
Helmand River below Kajakai Reservoir	1947–1980	http://waterdata.usgs.gov
Kajaki Reservoir		
Daily reservoir levels	1 Oct 2006–present	Personal communication, John Hazelton, USACE
Monthly reservoir levels	Apr 1998–Sep 2008	Personal communication, John Hazelton, USACE
Historical Daily Storage	1960–1980	Personal communication, John Hazelton, USACE
Elevation–Discharge Relationship		Personal communication, John Hazelton, USACE
Elevation–Storage Relationships; Design (1953), 1968, 2007		(Perkins and Culbertson 1970, Vining and Vecchia 2007)
Elevation–Area Relationship		(Perkins and Culbertson 1970, Blue 2006)
Meteorological Data		
Daily gage precipitation	2003–2009	Personal communication, USAID
Daily gage temperature	2003–2009	Personal communication, USAID
Daily gage evaporation	2003–2007	Personal communication, USAID
TRMM 3B42 Daily 0.25° gridded rainfall	1997–present	(Huffman et al. 2007)
Snow Covered Area (SCA)	2006–2009	(Daly et al. 2004–2010)
Snow water equivalent (SWE)		
SSM/I daily SWE	1987–present	(Armstrong and Brodzik 1995)
AMSR-E daily SWE	2002–present	(Kelly et al. 2003)
GIS Data		
Afghanistan 90 m SRTM DEM		(USGS 2000)
Soviet topographic map layers		(Chirico and Warner 2005)
Afghanistan political boundaries/locations—cities, provinces, districts, roads, etc		(AIMS 1997)
Afghanistan land type coverage		(AIMS 1997)
Afghanistan water layers—streams, canals, dams, etc.		Personal communication, Topographic Engineering Center (TEC), USACE

2.2.1 Hydrologic Data

2.2.1.1 Discharge Data

Several streamflow gages were in operation in Afghanistan prior to 1980 (USGS 1979). There is an ongoing effort to reinstall these gages to monitor flow, but as of this report, the Helmand River has no operational gages. Historical data are available until 1980 from three stations above the Kajakai Reservoir and one just downstream of the dam (Fig. 2-3). Historical flow records show a typical snowmelt fed system, with the highest flows occurring during the spring runoff.

2.2.1.2 Kajakai Reservoir Data

Daily storage values were reported at the reservoir between 1953 and 1980. These data were converted to elevations using elevation–storage relationships for the reservoir developed in 1953 and 1968 (Perkins and Culbertson 1970). In 2007, the USGS conducted a sedimentation study and developed an updated elevation–storage relationship (Vining and Vecchia 2007). Figure 2-5 shows the reduction in storage based on the 1953, 1968 and 2007 elevation–storage relationships. Monthly water surface elevations are available after 1998; and some daily data are available during the 2006–07 and 2008–09 water years. A relationship between water surface elevation and surface area was developed using high-resolution imagery (Blue 2006). However, the datum used does not match the local datum on which the other data are based, and, as of this report, this issue was still unresolved. The elevation–storage-area relationship used in this study is based on the most recent data available at the local datum (Table 2-2). See eq A1 for details on equation formats.

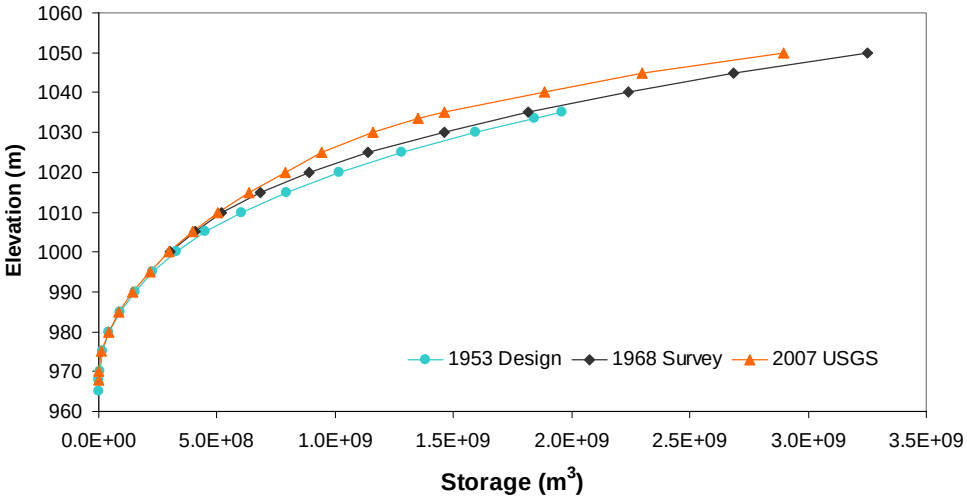

Figure 2-5. Storage–elevation relationships for the Kajakai Reservoir.

Table 2-2. Area-storage-elevation relationship for the Kajakai Reservoir.

Elevation (m)	Area (1000 m²)†	Storage (1000 m³)‡
970	712	2000
975	3899	13000
980	7801	42000
985	10300	87000
990	12840	145000
995	15504	216000
1000	17837	299000
1005	20980	395000
1010	28770	504000
1015	36554	633000
1020	46168	788000
1025	57302	941000
1030	67823	1160000
1035	77164	1459000
1040		1886000
1045		2299000
1050		2899000

†Perkins and Culbertson (1970)
‡Vining and Vecchia (2007)

Discharge from the reservoir was estimated using an elevation–discharge rating curve based on the spillway geometry, power production at the hydropower plant, and irrigation withdrawals (personal communication with John Hazelton, USACE, 2009). Two hydropower units (no. 1 and 3) were

assumed to be running at full capacity for the given reservoir level unless available data showed that they were shut down. Three jet valves were used to release water for irrigation. The operation of the jet valves changed seasonally; typically, the highest releases occurred during the spring run-off period, with minimal releases in the fall and winter. Actual jet valve operating procedures were unknown for the majority of the study time period. Estimated daily discharges for the periods in 2006–07 and 2008–09 when daily elevation data are available are shown in Figure 2-6.

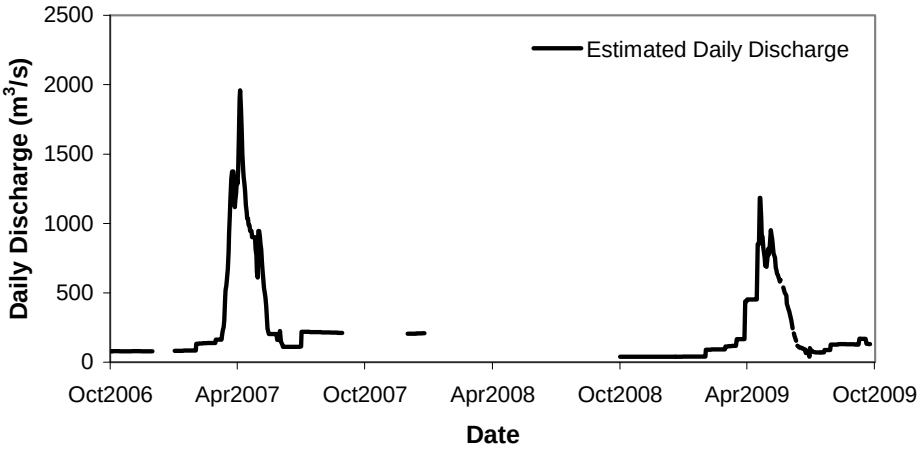

Figure 2-6. Estimated daily discharge from Kajakai Reservoir.

Inflows, *I*, to the Kajakai Reservoir were estimated by computing a complete reservoir water balance

$$I(t) = \frac{dS}{dt} + O(t) - P(t) + E(t), \quad (2)$$

where

dS/dt = change in storage over a given time
t = estimated using the reported water surface elevations and the elevation–storage relationship
O = discharge calculated from the discharge–elevation rating curve
P = precipitation
E = evaporation.

Precipitation and evaporation had minimal impact on the change in reservoir storage.

2.2.2 Precipitation

Ground observations of precipitation have been reported by the Afghan Agricultural Research Department–Meteorological Department at 126 stations across Afghanistan since 2003. Two gages lie within the Upper Helmand Watershed, and several more are adjacent to the basin (Fig. 2-7). Measurements are taken daily, though there are large data gaps at several stations. The data quality is also unclear. Limited documentation is available on collection methods, though the values generally agree with climatology data and weather accounts.

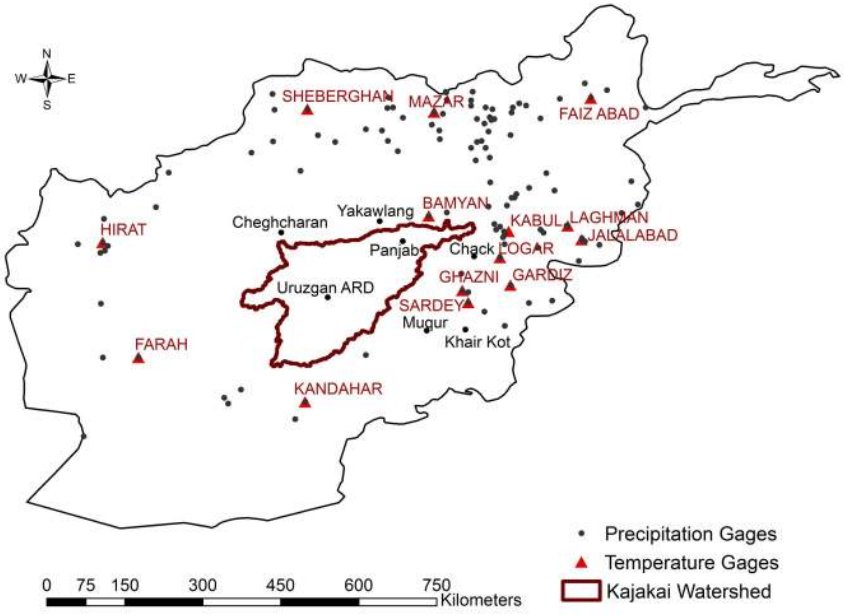

Figure 2-7. Locations of meteorological stations in Afghanistan.

Precipitation data are also measured remotely through the Tropical Rainfall Measuring Mission (TRMM) (Huffman et al. 2007). The TRMM remote measurements of precipitation are derived from two basic data sources: passive microwave and infrared. Passive microwave (PMW) sensors estimate precipitation by detecting, at high frequencies, the scattering of the Earth's radiation when rain is present in the atmosphere and, at low frequencies, the thermal energy from the rain. Infrared (IR) sensors measure outgoing longwave radiation to estimate cloud-top temperatures and position (Sapiano and Arkin 2009).

The TRMM 3B42 precipitation data are available from NASA's Goddard Earth Sciences (GES) Data and Information Services Center (DISC).

TRMM uses the AMSU-B, SSM/I, TMI, and AMSR-E passive microwave sensors (Huffman et al. 2007). Passive microwave signals are impacted by the presence of a snowcover and are therefore unreliable in detecting rainfall in snow-covered regions. Infrared data are calibrated to the passive microwave data to provide an independent estimate of precipitation. IR data are used to fill in gaps when passive microwave data are missing. The TRMM 3B42 product is a gage-corrected dataset available at 3-hour and daily time intervals. For this study, the daily products were used. TRMM data are available from January 1998 through the present and have a spatial resolution of $0.25 \times 0.25°$.

2.2.3 Temperature

Historical temperature data are available from the National Climatic Data Center at World Meteorological Organization (WMO) stations between 1973 and 1990. Between 2003 and 2009, a limited number of Afghan Agricultural Research Department-Meteorological Department stations provided daily temperature data, though none of the stations were within the Upper Helmand watershed (Fig. 2-7). Daily temperature grids over the basin were generated by interpolating the gage data using an inverse distance weighting method, and adjusting for elevation using a temperature lapse rate. The entire month of December 2006 is missing from all stations. To fill in this gap, average daily temperatures were calculated using the historical period of record.

The lapse rate was determined by fitting a linear regression to the average monthly temperatures, calculated from 2003–2009, by elevation. Figure 2-8 shows the average monthly temperature for each station plotted by elevation. Because the lapse rate did not vary by the month, a single average value of 5.6°C/km was used. The daily station temperature data were adjusted to sea level by

$$T_{0i} = T_i + 0.0056(E_i) \tag{3}$$

where

T_i = recorded temperature at the station i
T_{0i} = temperature at sea level
E_i = elevation of the station i in meters.

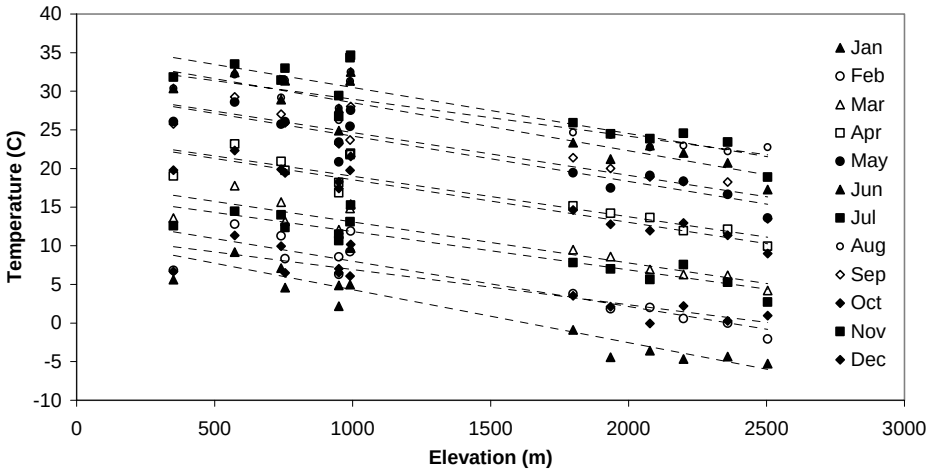

Figure 2-8. Average monthly observed temperatures, 2003–2009, by elevation.

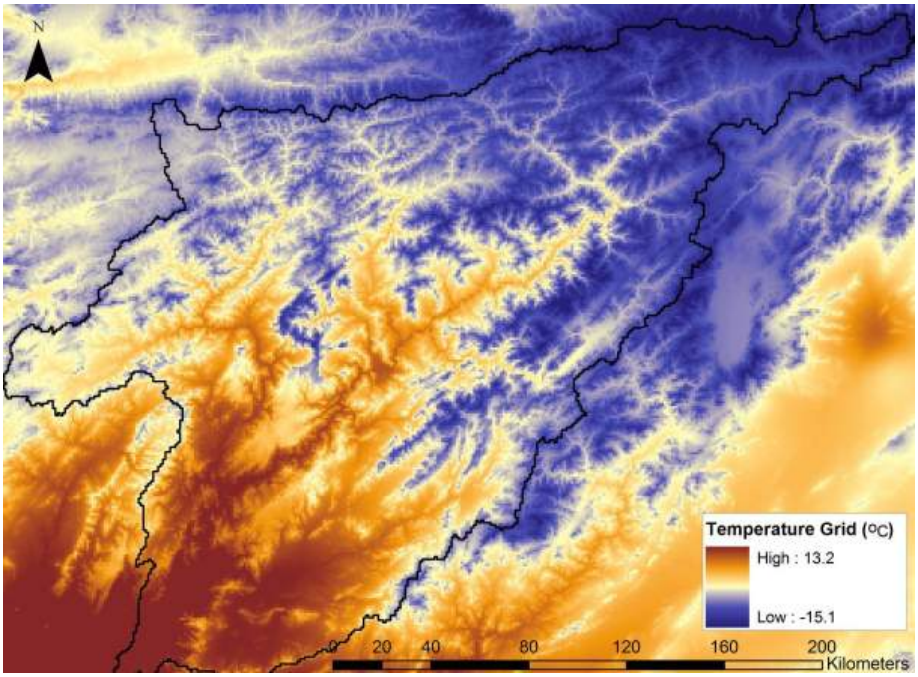

Figure 2-9. Example of interpolated 1-km temperature grid.

A 1-km grid covering the Upper Helmand basin was created by interpolating the sea level temperatures. The temperature at each pixel was then adjusted to the pixel elevation using

$$T_j = T_{0j} - 0.0056(E_j), \tag{4}$$

where

T_j = final temperature at the pixel j
T_{0j} = pixel temperature at sea level

E_j = elevation of the pixel j in meters.

The pixel elevations were obtained from a USGS 90-m digital elevation model (DEM) of Afghanistan. Figure 2-9 shows an example of an interpolated temperature grid over the Upper Helmand Basin.

2.2.4 Evaporation

Evaporation data are available from 2003 to 2006, with some limited measurements in 2007, at the Kandahar airport. To estimate evaporation during missing periods, a modified Hargreaves equation was used. The Hargreaves equation can be used to estimate evaporation when only temperature data are available (Maidment 1993)

$$E_o = CS_o(T + 17.8)\sqrt{T_{\max} - T_{\min}} \tag{5}$$

where

E_o = evaporation (mm/day)
C = empirical coefficient for the region
S_o = solar radiation (mm/day)
T_{max} = mean monthly maximum temperature (°C)
T_{min} = mean monthly minimum temperatures (°C)
T = average daily temperature (°C).

Kandahar is located 100 km to the southeast of the Kajakai Reservoir at approximately the same elevation, 1000 m. Because of its location further south, it is likely that the weather is warmer at the Kandahar station than at the reservoir.

The Hargreaves method, developed from a study of fescue grass in Davis, CA, typically uses a value of 0.0023 for C. For the Afghan study region, this coefficient consistently underestimated the measured evaporation data. By use of the daily evaporation measurements, C values were calculated and the average C value, 0.0042, was used in this study. The calculated evaporation had a bias and RMSE of –0.6 and 2.9 mm, respectively, and an R^2 value of 0.533. Figure 2-10 shows the calculated evaporation using the modified Hargreaves method and the measured values at the Kandahar Station.

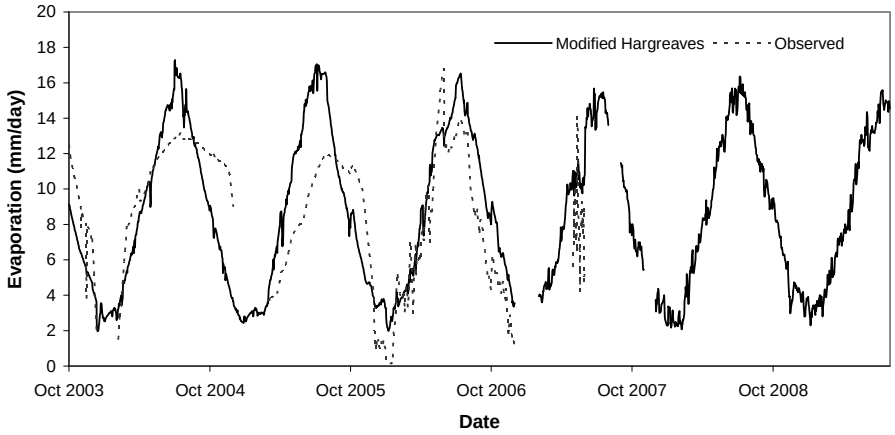

Figure 2-10. Calculated and observed evaporation at the Kandahar Airport

2.2.5 Snow covered area

Biweekly SCA images, created for operational snow assessments of Afghanistan (Daly et al. 2004–2010), were available during the winter seasons of 2006–07, 2007–08, and 2008–09. The majority of the images were created using the Advanced Very High Resolution Radiometer (AVHRR) imagery, though some were created using the Moderate Resolution Imaging Spectroradiometer (MODIS) imagery. The images were processed to mask out any cloud covered areas. The resulting SCA grids have a 1-km resolution, with each pixel classified as snow, no snow, or cloud covered.

2.2.6 Passive Microwave SWE

Daily passive microwave SWE data were available from two sources: the Advanced Microwave Scanning Radiometer–Earth Observing System (AMSR-E), and the Special Sensor Microwave/Imager (SSM/I). AMSR-E was launched on NASA's Aqua satellite in 2002 and calculates SWE based on brightness temperatures measured at wavelengths 19.7 and 36.5 GHz, with a spatial resolution of 28 × 16 km (19.7 GHz) and 14 × 8 km (36.5 GHz) (Kelly et al. 2004). AMSR-E SWE is available from the National Snow and Ice Data Center (NSIDC) in Equal-Area Scalable Earth (EASE)-grid projection as 25-km grids.

The SSM/I sensor was launched in 1987 on board the Defense Meteorological Satellite Program (DMSP) satellites. These data are available in near real-time and have the advantage of a long historical record. SWE estimates are derived from the SSM/I brightness temperatures measured at wavelengths 19 and 37 GHz, and have a spatial resolution of 69 × 43 km

(19.4 GHz) and 37 × 29 km (Armstrong and Brodzik 1995). The data are also available from NSIDC in an EASE-grid projection at a 25-km resolution.

SSM/I and AMSR-E global SWE products are available twice daily: ascending passes that occur in the afternoon and descending passes that occur in the early morning. For this study, only descending SWE data were used to reduce the potential wet snow effects in the afternoon. A gap in the satellite swath coverage over the region of interest occurs every 3 to 4 days. The SSM/I and AMSR-E gridded SWE data were converted to geoTiff format and re-projected to an Albers Equal Area projection. The grids were resampled to 1-km grid cells using the Nearest Neighbor method, which assigns the same value to the pixel as the data layer in that location without any interpolation. The basin-average SWE was calculated over the Upper Helmand watershed and 11 subbasins for each day on which no grid cell values were missing. To reduce the scatter present in the daily data, the maximum weekly values were extracted.

2.2.7 GIS Data

GIS layers of the study region were acquired from several sources. A 90-m digital elevation model (DEM) was obtained from the USGS (2000). Topographic maps developed by the Soviets in the late-1980s were also obtained through the USGS (Chirico and Warner 2005). Landuse shapefiles were obtained from the Afghanistan Information Management Services (AIMS 1997). All data layers obtained and created were projected to an Albers equal-area projection, centered on Afghanistan. A list of the GIS layers and projection information appears in Appendix A.

2.3 Modeling

A snow hydrology model of the Upper Helmand Watershed and subbasins was developed and validated using historical data and recent measurements at the Kajakai Reservoir. The Hydrologic Modeling System (HMS), developed by the Hydrologic Engineering Center (HEC), computes a complete water balance of a basin to estimate streamflow given precipitation input (USACE 2009). HMS is designed for a variety of water resource applications and can be adapted to specific watershed characteristics. Several options are available for modeling each aspect of the hydrologic process. HMS can be run as a lumped-parameter or distributed model. The lumped-parameter approach uses point data to estimate average values

over a specified area. The distributed approach models the basin on a user-defined grid, estimating values at each grid cell.

HMS includes a temperature index snow model that calculates SWE given temperature and precipitation data. Given the limited data available in Afghanistan, a temperature index snow model was considered appropriate for this study. The snow model in HMS is an adaptation of over 50 years of snow modeling efforts in the Corps of Engineers going back to the Cooperative Snow Investigation Program (USACE 1956). Recent developments allow the snow model to be used in the HMS distributed model to calculate snowmelt at each grid cell (Daly et al. 1999). The distributed approach to modeling snow allows watershed heterogeneity to be represented and remote sensing data to be directly compared.

A distributed HMS model was developed for the Upper Helmand Watershed. The snow model was run from October through June for six winter seasons, 2004–2009, to capture the entire snow accumulation and ablation period. The daily precipitation and temperature grids required as input to the model were described in Sections 2.2.2 and 2.2.3, respectively. The following sections describe the model development, including selected approaches and parameter estimation.

2.4 Watershed Physical Description

The physical representation of the watershed for the HMS model was developed using the spatial hydrology tool, GeoHMS, within ArcGIS. Basin characteristics were derived from the USGS DEM for each subbasin (Table 2-3). GeoHMS was also used to create the HMS grid-cell file, required to run the model in distributed format. The grid-cell file is used by the model to route the runoff in each cell to the basin outlet. For each subbasin, the file lists each grid cell within the subbasin, the coordinates of the cell, the fraction of area of the cell located in that subbasin, and the downstream distance to the subbasin outlet. All gridded input data to the model were formatted to match the coordinate system of the grid-cell file.

Table 2-3. Basin physical characteristics.

Subbasin	Area (km^2)	Longest flow path (km), L_L	Length to centroid (km), L_C	Average elevation (m)	Slope (km/km)	Time of concentration (hr), t_c	Storage coefficient (hr)
1	4884	187.5	73.2	3268	0.011	21.1	31.7
2	2458	102.6	50.6	3197	0.019	10.7	16.0
3	8444	198.0	85.7	2747	0.014	20.0	30.0
4	4744	206.2	114.2	2278	0.009	24.6	36.9
5	4385	187.6	83.6	2384	0.014	19.5	29.2
6	5301	185.3	116.7	2503	0.010	21.9	32.8
7	2354	133.4	69.6	2287	0.011	16.5	24.8
8	4017	169.7	46.7	2332	0.014	17.6	26.5
9	8238	230.9	96.1	2201	0.010	25.7	38.6
10	538	59.4	21.3	1533	0.016	7.5	11.2
11	1320	73.9	34.9	1372	0.011	10.3	15.4
Entire Basin	46683	510.5		2630	0.005		

2.5 Temperature Index Snow Model

In the HMS snow model, snow accumulates when precipitation falls and the air temperature is below a rain/snow discriminating temperature, T_{PX}, typically set equal to freezing. The temperature of a snowpack varies over time owing to energy transfer between the snowpack and the surrounding air. The temperature gradient within the snowpack and the air temperature determine whether the energy exchange is positive or negative. During periods of lower air temperatures, the snow is cooled as heat from the snowpack is released into the air. When the air is warmer, heat is transferred into the snowpack, warming it to a maximum of 0°C.

As the air temperature rises above freezing, two conditions must be met before melt can occur. The cold content of the snowpack must be depleted and the liquid water deficiency must be filled. The cold content, *cc*, is defined as the amount of liquid water required to raise the temperature of the snowpack to 0°C, given by

$$cc = \frac{\rho_s C_p d(\Delta T_s)}{\rho_w L_f} = \frac{SWE \cdot C_p(\Delta T_s)}{L_f} \tag{6}$$

where

cc = cold content (mm)
ρ_s = density of snow (kg/m^3)
C_p = specific heat of ice (J/kg-°C)
d = snow depth (mm)
ΔT_s = difference between the average snowpack temperature and the base temperature (°C)
ρ_w = density of water (kg/m^3)
L_f = latent heat of fusion (kJ/kg).

The average snowpack temperature is unknown and is calculated based on work of Anderson (2006) by estimating the heat transfer within the snowpack and from the snowpack to the air and ground using a snow temperature index, *ATICC*

$$ATICC_2 = ATICC_1 + \left(1-\left(1-C_{ATICC}\right)^{days}\right)\cdot\left(T_a - ATICC_1\right) \quad (7)$$

where
$ATICC_2$ = antecedent temperature index for the current timestep
$ATICC_1$ = index from the previous timestep
C_{ATICC} = weighting parameter which determines how much earlier estimates of ATICC impact the current value
$days$ = timestep length in days.

For this study, a C_{ATICC} of 0.84 gave the best results during calibration. In the model, the snowpack properties and rate of change in cold content are represented by a cold rate parameter, c_{CR}, so the equation for cold content becomes

$$\Delta cc = c_{CR}\left(T_a - ATICC\right) \quad (8)$$

Cold content accumulates over the winter during periods of sub-freezing temperatures. As liquid water enters the snowpack from melt or rain, initially that water will freeze, thereby releasing heat into the snow and decreasing the cold content. When the entire snow depth is at an isothermal 0°C, the cold content is zero. Before runoff can occur, the storage capacity of the snowpack, known as the liquid water capacity, LW_{cap}, must also be filled. This value is given as a percentage of the snowpack, typically 2–5%.

Snow can melt at two interfaces: at the snow–ground interface and the snow–air interface. At the ground surface, model snowmelt is given either as a constant value, or a constant monthly value. At the air interface, the basic equation for snowmelt, M, in a temperature index model is

$$M = c_{MR}\left(T_a - T_b\right) \tag{9}$$

where

c_{MR} = melt rate coefficient
T_a = air temperature
T_b = base temperature at which snow melts, typically 0°C.

Different melt rate coefficients are used for dry conditions versus rain conditions.

The dry melt rate coefficient is a function of a degree-day index, which allows the rate to change during the season as the albedo and density of the snow change. The degree-day index at the current time step, $ATIMR_2$, is calculated as

$$ATIMR_2 = (T_a - T_b) + K^{days}(ATIMR_1) \cdot days \tag{10}$$

where

K = ATI-meltrate coefficient, typically set to 0.98
$ATIMR_1$ = degree day index from the previous timestep.

During rainy conditions, snowmelt occurs at a faster rate because heat from the liquid precipitation warms the snowpack. Melt can be solved directly by making several assumptions (USACE 1956):

- Shortwave radiation is minimal because of cloud cover.
- Longwave radiation can be adequately indexed by air temperature as cloud temperature is likely reasonably similar.
- Humidity is near 100%.
- Wind is minimal beneath a forest canopy, though in open areas it may impact model results.

The equation for the melt rate coefficient during rain events then becomes:

$$C_{MR} = R_{MR} + 0.007P \tag{11}$$

where

R_{MR} = wet melt rate (mm/°C-day)

P = precipitation (mm).

A value of 3.3 mm/°C-day was used in the model, based on calibration and suggested values (USACE 1998).

The snow model was sensitive to the input temperature grids. Initially, a typical lapse rate was used. When the temperature grids were generated using the lapse rate calculated from the Afghanistan temperature station data, the results improved considerably. The melt rate also had an effect on model results, to a much lesser degree, and was adjusted during calibration. Changing the other parameters did not notably impact the model results. All parameter values used in the snow model are given in Table 2-4.

Table 2-4. Snow parameters used in the temperature index snow model.

Snow Model Parameter		Value
Snow/Rain Discriminating Temperature	T_{PX}	0°C
Snowmelt Temperature	T_{BASE}	0°C
Wet Meltrate	R_{MR}	3.3 mm/°C-day
Rain Rate Limit	L_{rain}	1 mm/day
Antecedent Temperature Index-Meltrate Coefficient	K	0.98
Cold Limit	L_{snow}	20 mm/day
Antecedent Temperature Index-Coldrate Coefficient	C_{ATICC}	0.84
Liquid Water Capacity	LW_{cap}	5%
Groundmelt Rate	R_{GM}	0.025 mm/day

Antecedent Temperature Index, *ATI* (°C-day)	Meltrate, $c_{MR\text{-}dry}$ (mm/°C-day)	Coldrate, c_{CR} (mm/°C-day)
0	1.09	1.22
38	1.32	1.32
93	1.78	1.32
1000	1.78	1.32

2.6 Hydrologic Model

Model parameters for baseflow and routing were developed using historical discharge data from three stream gages on the upper Helmand River during dry, non-snowmelt periods. Unit hydrograph parameters were estimated using the basin physical characteristics. Initial model parameters

for infiltration were estimated assuming a sandy soil and adjusted until the modeled inflow time series agreed with the computed inflow time series during the 2006–07 winter season. The model was then run for the remaining years of data.

2.6.1 Baseflow

The baseflow, Q_t, at a given time was modeled using the recession method, which describes the decrease in baseflow over time as an exponential decay, as

$$Q_t = Q_0 K^t \tag{12}$$

where

Q_o = initial baseflow discharge following an event
K = recession constant
t = time (days).

Discharge data from 1953 to 1979 on the Helmand River at Dehraut were used to estimate K. The receding flow values from May, June, and July for each year gave an average recession constant of 0.97. Spring runoff had a more rapid recession with K = 0.94.

The initial baseflow discharge was determined by weighting discharge by watershed area. The baseflow on the first of July was assumed to represent a typical baseflow conditions. The scaled average discharges on the first of July at Dehraut and Gizab were 0.002 m^3/s per km^2 and 0.0035 m^3/s per km^2, respectively. The Gizab baseflow was used for subbasins 1–4. The Dhraut baseflow was used for all other subbasins.

2.6.2 Loss

The Deficit and Constant method was chosen to account for losses ascribable to soil infiltration. This method continuously accounts for soil moisture by using potential evapotranspiration data. Monthly average evapotranspiration values were calculated for each subbasin using the Hargreaves method (Section 2.2.4) with basin average temperatures adjusted for elevation. Table 2-5 lists the loss parameters used in the model.

Table 2-5. Deficit and constant loss parameters.

Parameter	Model Value
Initial Deficit	1.0 mm
Maximum Deficit	40 mm
Constant Rate	0.5 mm/hr
Impervious	15%

2.6.3 Surface Runoff

A distributed version of the Clark method, ModClark, was used to transform the excess water in each grid cell to stream runoff. The Clark method develops a synthetic unit hydrograph based on watershed characteristics. This method requires a time of concentration and a storage coefficient for each subbasin. The time of concentration, t_c, was estimated using the Kirpich method (Kirpich 1940)

$$t_c = 3.97 L_L^{0.77} S^{-0.385} \tag{13}$$

where

t_c = time of concentration (minutes)
L_L = longest flow path length (km)
S = average slope (m/m).

The ratio of the storage coefficient to the time of concentration is typically constant over a region. A ratio of 1.5 was determined by calibration to give the best results. Table 2-3 gives the ModClark parameters used in the model.

2.6.4 Routing

The Muskingum method was used to route the stream flow through each reach. This method is based on the principle of mass conservation, which states that the rate of change of storage within a reach must equal the difference between the inflow and outflow to the reach. The Muskingum method is described by the formula

$$S = K\left[XI + (1 - X)Q\right] \tag{14}$$

where

S = storage within the reach
I = inflow
Q = outflow
X = weighting factor which describes the type of storage within the reach
K = coefficient that represents the time it takes the flood wave to travel through the reach.

Historical discharge data at two stations along the Helmand River, Gizab and Dehraut, were used to calibrate the Muskingum coefficients used in the model. The data at both gages were normalized by watershed area and the estimated baseflow was subtracted to compare the inflow and outflow hydrographs. Figure 2-11 shows the actual inflow and outflow hydrographs for a runoff event in July of 1978, and the modeled outflow. The timing and magnitude of the outflow hydrographs match well, with a Nash-Sutcliffe efficiency of 0.89. By use of this method, the values for X and K were determined to be 0.25 and 0.65 days, respectively. These values agree with values used in a historical modeling effort in the watershed (Harza 1976), which found X to be 0.25 and K to range between 0.15 and 0.64 days. However, to match the timing of the discharge peaks, K was increased to 1.5 days during model calibration.

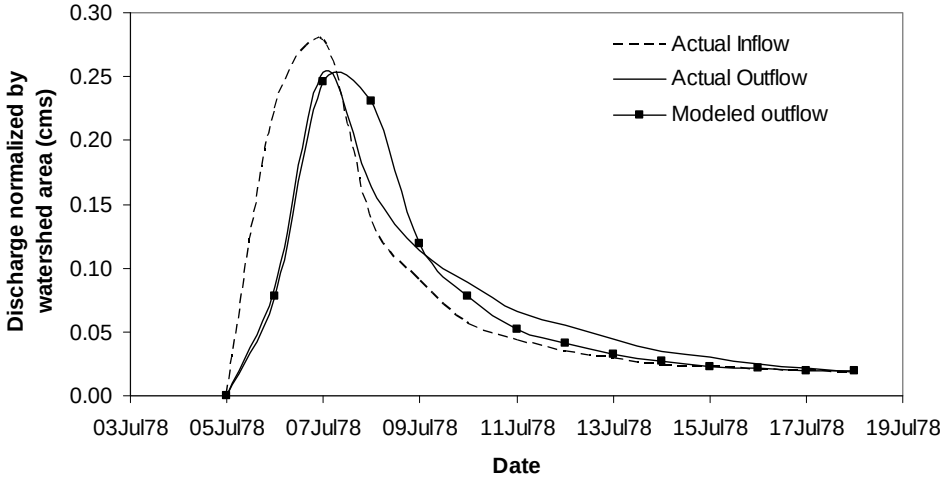

Figure 2-11. Results of Muskingum parameter calibration for runoff prediction at Dehraut.

2.7 Model calibration

The modeled snow extent was compared to high-resolution SCA imagery available from 2006–2009. The SCA comparison indicates whether the

model was correctly simulating snow accumulation and melt throughout the season. Daily water level observations available during the 2006–07 and 2008–09 winter seasons were used to estimate reservoir inflows using the method described in Section 2.2.1.2. The model was then run for the remaining five winter seasons, 2004–2009.

3 Results

This chapter is broken into three sections. The first section describes the preliminary analysis of the study data and methods. An overview of the basin hydrology is given. The second section describes the snow modeling results. The modeled snow extent is compared to the high-resolution SCA imagery and the modeled SWE is compared to passive microwave estimates of SWE. Finally, the third section presents the hydrologic model results in which the model's results are compared to reservoir observations.

3.1 Preliminary Results

3.1.1 TRMM and gage precipitation comparison

To evaluate the remotely sensed TRMM data, the TRMM precipitation estimates were compared to gage measurements in the study region. Pixel values that coincided with each gage location were extracted from the TRMM precipitation grids for each day during the period of record. The daily precipitation data were accumulated monthly and over each winter season, October–June. The data were compared annually, by month and by station. Each TRMM pixel value covers a 25-km^2 area in comparison to the diameter of the point gage measurement. While the data should be reasonably similar without any obvious biases, the satellite estimates are not expected to match the gage measurements exactly. Errors associated with both ground measurements (e.g., undercatch due to wind), and satellite data (e.g., effects of land type, gaps in satellite coverage) will cause the results to differ. In addition, TRMM retrievals may degrade when snow is present. Based on the gage data, 95% of the annual precipitation falls during the study period, October–June, when a snowcover is expected to be present.

A comparison of TRMM 3B42 satellite precipitation and gage measurements found that TRMM reasonably matches the timing and volume of precipitation over the Upper Helmand watershed. The seasonally accumulated TRMM precipitation consistently underestimates the gage precipitation, particularly during the greatest precipitation observations (Fig. 3-1), but this might be attributable to the large pixel area over which the data are averaged. A statistical analysis of the monthly accumulated precipitation is given in Table 3-1. Some stations had higher correlations than oth-

ers, though no discernible pattern is evident based on location or elevation. Some months had better correlations than others, but not in a temporal pattern that would suggest that TRMM does not measure precipitation well during the winter months when a snowcover is present. Two years, 2003–04 and 2005–06, had noticeably lower precipitation than the other years, based on both TRMM and gage measurements. The year with the greatest amount of precipitation was 2006–07.

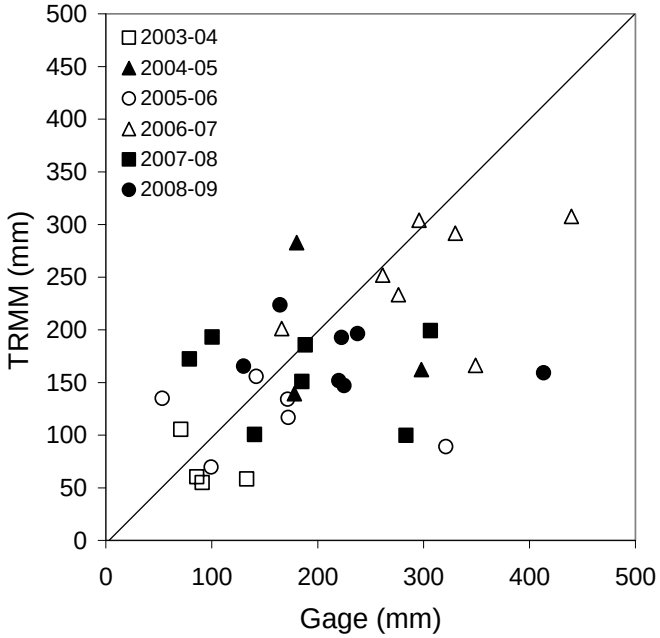

Figure 3-1. Accumulated winter season precipitation, TRMM and Gage measurements.

Table 3-1. Comparison of TRMM and Gage monthly accumulated precipitation, 2003–2009.

Station	Elevation (m)	R^2	Month	Average accumulated TRMM precip. (mm)	Average accumulated gage precip. (mm)	R^2
Chack	2185	0.396	Oct	1.55	0.91	0.001
Cheghcharan	2230	0.241	Nov	12.97	25.69	0.189
Khair Kot	2120	0.132	Dec	23.93	30.85	0.233
Muqur	2000	0.517	Jan	33.93	41.92	0.241
Panjab	2710	0.511	Feb	30.33	50.63	0.268
Uruzgan	1760	0.383	Mar	31.83	57.88	0.152
Yakawiang	2583	0.336	Apr	22.69	33.34	0.523
Jaghatoo	580	0.459	May	12.92	15.18	0.002
Zabul	2503	0.212	Jun	9.67	10.05	0.243
All data monthly						0.247

3.1.2 Reservoir Inflow Analysis

During the study period, 2003–2009, no streamflow data were measured. The reservoir water balance (eq 2) was used to estimate watershed outflows (inflows to the reservoir). To validate this approach, inflows were simulated for the historical period, 1953 to 1979, when discharge data were available, using the same method. Historical daily storage data for the Kajakai Reservoir were converted to elevation using the elevation–storage relationships from 1953 and 1968 (Fig. 2-5). Precipitation and evaporation were not available for the historical period. However, because they were small relative to other inflows and outflows, they were neglected. The three irrigation jet valves were assumed to be 30% open for the entire year as actual irrigation withdrawals are unknown during this time. Two generating units were assumed to be running at 100% once the Kajakai Dam began power generation in 1975. Discharge for both irrigation and power generation were determined as a function of reservoir elevation.

The calculated inflow was compared to historical Helmand River discharge data at Dehraut, which is located approximately 12 km upstream of the reservoir (Fig. 3-2). To evaluate the results, a Nash-Sutcliffe efficiency, *E*, was calculated by

$$E = 1 - \frac{\sum_{i=1}^{n} (O_i - M_i)^2}{\sum_{i=1}^{n} (O_i - \overline{O})^2} \tag{15}$$

where

O_i = observed value

M_i = model value at time *I* (Nash and Sutcliffe 1970).

E can range from 1 to –∞, with an efficiency close to 1 signifying a strong fit between the modeled and observed values and a negative value indicating that the average observed value would lead to better results than the model. The calculated inflows match the gage data well, with a Nash-Sutcliffe efficiency of 0.78. Peak flows are particularly well simulated. During the late-spring through early winter periods, when inflows are lower, discharges do not match as well. This discrepancy is likely because of assumptions made regarding the irrigation withdrawals, which are typically greater than 30% during the spring runoff and zero in the early winter pe-

riod. Overall, this method simulates inflows to the reservoir well during the most crucial peak flows.

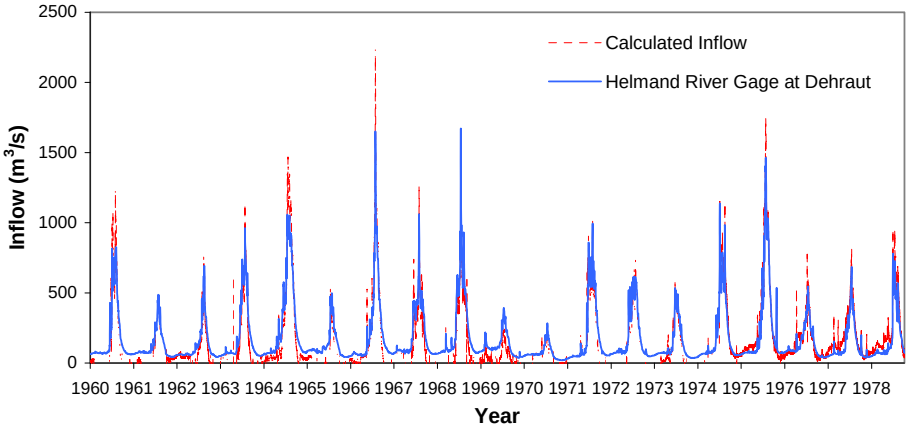

Figure 3-2. Comparison of calculated and gage inflows to Kajakai Reservoir.

3.1.3 AMSR-E and SSM/I Comparison

The weekly average basin SWE depths, extracted from the SSM/I and AMSR-E datasets, were compared. The analysis over the Upper Helmand watershed indicates that the two datasets are quite similar, with a correlation of 0.94 (Fig. 3-3). Despite the scatter, the daily average basin SWE has a correlation of 0.91 and a Nash-Sutcliffe efficiency of 0.87. Both estimates of SWE consistently increase during the snow accumulation period and display more scatter during the snowmelt period. The primary difference is that the AMSR-E sensor detects SWE earlier in the winter and later in the spring, which may indicate that AMSR-E is better at detecting shallow snowpacks than the SSM/I sensor. The subbasin SWE values also compared well between AMSR-E and SSM/I. Table 3-2 gives the maximum annual subbasin SWE for AMSR-E and the correlation between AMSR-E and SSM/I for all years. The average SWE depth is greatest in mountainous subbasins 1 and 2, which also have the highest correlations. The greatest volume of SWE comes from subbasin 3, which is also located in the mountainous region and has the largest subbasin area. For this study, AMSR-E was used because of its higher resolution, but for a large watershed comparison both datasets give approximately identical results. This allows the use of the longer historical record of SSM/I SWE to analyze snowpack trends in the basin.

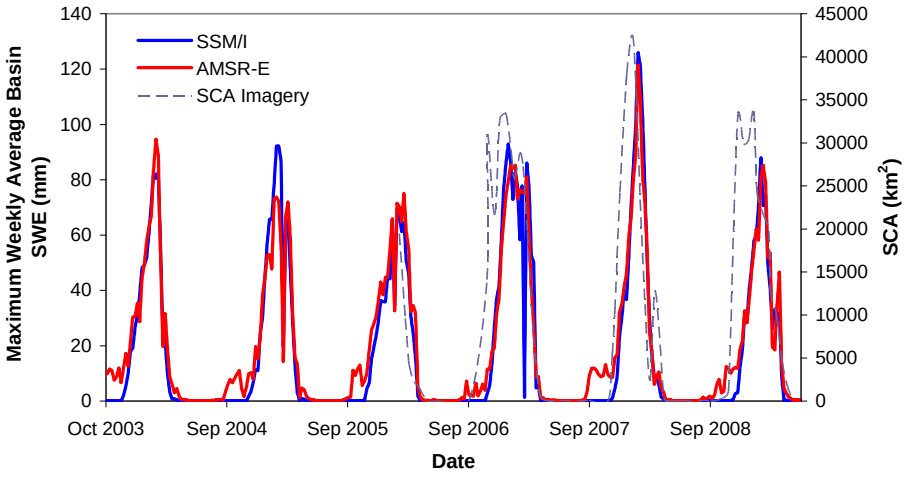

Figure 3-3. Comparison of SSM/I and AMSR-E weekly maximum SWE depth, showing SCA.

Table 3-2. AMSR-E Maximum annual basin-average SWE depth (mm) and correlation with SSM/I.

Basin	2003–04	2004–05	2005–06	2006–07	2007–08	2008–09	R^2 for AMSR-E and SSM/I, all years
Subbasin 1	212	161	176	180	175	160	0.92
Subbasin 2	214	147	178	167	181	181	0.91
Subbasin 3	124	121	116	133	160	121	0.92
Subbasin 4	136	121	106	113	173	144	0.89
Subbasin 5	27	69	17	35	66	32	0.80
Subbasin 6	128	100	92	130	175	139	0.85
Subbasin 7	76	83	57	110	157	99	0.78
Subbasin 8	25	49	14	68	64	31	0.77
Subbasin 9	26	56	22	34	51	30	0.85
Subbasin 10	7	11	5	4	16	1	0.37
Subbasin 11	11	11	10	6	16	7	0.15
Upper Helmand Watershed	95	74	75	85	121	85	0.92

3.1.4 Upper Helmand Basin Summary

The Upper Helmand watershed in Afghanistan is unique in many respects, and this is the first study to use remote sensing to analyze the snow hydrology in this region. This section presents a summary of the hydrologic conditions in the Upper Helmand basin (Table 3-3). This region is dry for much of the year. Precipitation begins increasing in November and continues through May, with the heaviest precipitation occurring in March.

Less than 5% of the total annual precipitation falls during the rest of the year. Over the 6 years of the study period, the accumulated annual precipitation, based on TRMM data, ranged from 100–300 mm. This is less than typically reported in climatology data, which estimates an annual precipitation between 200–400 mm.

Table 3-3. Annual hydrologic states derived from model results by basin.

	2003–04	2004–05	2005–06	2006–07	2007–08	2008–09
Upper Helmand Watershed						
Total accumulated precipitation (mm)	89	216	117	311	180	209
% Runoff from snowmelt	25	30	24	25	52	27
Average inflow (m^3/s)	114	245	89	418	177	206
Date of maximum SWE	15 Feb 04	26 Feb 05	31 Jan 06	18 Mar 07	15 Feb 08	22 Feb 09
Date of peak runoff	30 Jan 04	20 Mar 05	22 Feb 06	22 Mar 07	10 Jan 08	15 Apr 09
Subbasin 1						
Total accumulated precipitation (mm)	90	199	125	275	229	181
% Precipitation as snow	42	45	37	49	50	46
Average basin outflow (m^3/s)	6	14	9	31	18	13
Date of maximum SWE	19 Feb 04	7 Mar 05	5 Feb 06	18 Mar 07	25 Feb 08	1 Mar 09
Date of peak runoff	10 Mar 04	17 Mar 05	25 Mar 06	1 Apr 07	22 Apr 08	23 Mar 09
Subbasin 2						
Total accumulated precipitation (mm)	85	195	119	252	186	157
% Precipitation as snow	45	45	40	48	62	40
Average basin outflow (m^3/s)	4	9	5	16	9	8
Date of maximum SWE	19 Feb 04	4 Mar 05	4 Feb 06	18 Mar 07	24 Feb 08	1 Mar 09
Date of peak runoff	9 Mar 04	18 Mar 05	9 Apr 06	31 Mar 07	11 Apr 08	11 Apr 09
Subbasin 3						
Total accumulated precipitation (mm)	75	191	107	269	181	231
% Precipitation as snow	41	35	31	37	68	41
Average basin outflow (m^3/s)	12	26	11	51	17	31
Date of maximum SWE	17 Feb 04	25 Feb 05	4 Feb 06	18 Mar 07	17 Feb 08	23 Feb 09
Date of peak runoff	16 Nov 03	16 Mar 05	29 Apr 06	31 Mar 07	11 Apr 08	23 Mar 09
Subbasin 4						
Total accumulated precipitation (mm)	101	201	112	303	185	204
% Precipitation as snow	34	23	26	29	63	31

	2003–04	2004–05	2005–06	2006–07	2007–08	2008–09
Average basin outflow (m^3/s)	7	26	8	41	11	17
Date of maximum SWE	15 Feb 04	25 Feb 05	4 Feb 06	18 Mar 07	17 Feb 08	22 Feb 09
Date of peak runoff	9 Mar 04	16 Mar 05	19 Feb 06	19 Mar 07	6 Mar 08	12 Apr 09
Subbasin 5						
Total accumulated precipitation (mm)	60	192	90	294	173	217
% Precipitation as snow	16	23	17	12	48	16
Average basin outflow (m^3/s)	6	18	6	33	20	19
Date of maximum SWE	11 Feb 04	22 Feb 05	31 Jan 06	18 Mar 07	15 Feb 08	12 Feb 09
Date of peak runoff	16 Nov 03	16 Mar 05	1 Feb 06	19 Mar 07	8 Jan 08	14 Jan 09
Subbasin 6						
Total accumulated precipitation (mm)	109	222	154	371	156	203
% Precipitation as snow	31	28	26	31	59	28
Average basin outflow (m^3/s)	8	36	14	58	11	16
Date of maximum SWE	15 Feb 04	26 Feb 05	4 Feb 06	15 Mar 07	17 Feb 08	22 Feb 09
Date of peak runoff	7 Apr 04	15 Mar 05	18 Feb 06	18 Mar 07	15 Apr 08	12 Apr 09
Subbasin 7						
Total accumulated precipitation (mm)	55	171	137	416	119	189
% Precipitation as snow	24	40	38	25	59	23
Average basin outflow (m^3/s)	2	13	5	41	5	9
Date of maximum SWE	10 Feb 04	25 Feb 05	31 Jan 06	5 Mar 07	16 Feb 08	22 Feb 09
Date of peak runoff	17 Apr 04	15 Mar 05	9 Apr 06	18 Mar 07	9 Dec 07	15 Apr 09
Subbasin 8						
Total accumulated precipitation (mm)	107	203	110	408	181	202
% Precipitation as snow	7	17	12	6	37	8
Average basin outflow (m^3/s)	17	20	9	66	25	21
Date of maximum SWE	12 Feb 04	26 Feb 05	31 Jan 06	3 Mar 07	15 Feb 08	7 Feb 09
Date of peak runoff	28 Jan 04	15 Mar 05	31 Jan 06	18 Mar 07	8 Jan 08	14 Jan 09
Subbasin 9						
Total accumulated precipitation (mm)	94	301	121	306	191	235
% Precipitation as snow	16	32	17	18	42	23
Average basin outflow (m^3/s)	25	66	14	51	42	46
Date of maximum SWE	11 Feb 04	26 Feb 05	25 Jan 06	15 Mar 07	15 Feb 08	21 Feb 09

	2003–04	2004–05	2005–06	2006–07	2007–08	2008–09
Date of peak runoff	29 Jan 04	19 Mar 05	22 Apr 06	1 Apr 07	8 Jan 08	14 Jan 09
Subbasin 10						
Total accumulated precipitation (mm)	146	191	65	334	160	225
% Precipitation as snow	0	5	2	0	10	0
Average basin outflow (m^3/s)	8	4	2	16	8	10
Date of maximum SWE	3 Jan 04	26 Jan 05	20 Jan 06	23 Jan 07	3 Feb 08	20 Jan 09
Date of peak runoff	28 Jan 04	18 Mar 05	21 Nov 05	17 Nov 06	8 Jan 08	14 Jan 09
Subbasin 11						
Total accumulated precipitation (mm)	122	183	87	219	135	186
% Precipitation as snow	1	5	3	0	17	2
Average basin outflow (m^3/s)	17	11	5	19	10	14
Date of maximum SWE	1 Feb 04	14 Feb 05	9 Jan 06	24 Jan 07	10 Feb 08	24 Jan 09
Date of peak runoff	28 Jan 04	29 Dec 04	31 Jan 06	24 Feb 07	8 Jan 08	25 Jan 09

Snow begins accumulating in late October or early November and reaches a maximum extent by January, covering approximately 70% of the basin. Snow continues to accumulate at the higher elevations and generally reaches an average maximum SWE of 90 mm in late February. The melt period typically begins in late February or early March and continues through June. Snowmelt represents 25–50% of the total basin runoff. The percentage of runoff from snowmelt is greatest (50%) in the subbasins at the highest elevations, and less than 10% for the basins near the outlet.

Discharge typically begins increasing in late February or early March and continues through July, with the peak occurring around 15 April. Based on the historical discharge data at Dehraut, the average annual inflow to the Kajakai Reservoir is 177 m^3/s, and the average peak inflow to the reservoir is 900 m^3/s. For the remainder of the year (August–February), the inflow is 75 m^3/s, on average.

3.2 Snow Model Results

The model output SWE grids were spatially compared to remotely sensed SCA and SWE. The first analysis, a comparison to SCA imagery, tests the models ability to correctly estimate the snow extent throughout the winter season. The second analysis compares the model SWE to AMSR-E SWE,

both spatially and throughout the winter. The daily model results were averaged over the entire basin and each subbasin to obtain a time series of basin average SWE.

3.2.1 SCA Comparison

The total snow covered area estimated by the model was compared to the SCA imagery at approximately bi-weekly intervals throughout the 2006–07, 2007–08, and 2008–09 winter seasons. The high-resolution SCA imagery is considered to be the reference dataset, or "observation," of the snowcover extent because of its high accuracy. Visually, the time series of snow covered area closely resemble each other from October to June and compare particularly well during the snow accumulation and melt period (Fig. 3-4). In 2006–07 and 2007–08, the modeled snow extent overestimates the peak SCA. The time series have a correlation of 0.86, a Nash-Sutcliffe efficiency of 0.78, and a bias of 2232 km^2, or less than 5% of the total basin area, over the three winter seasons.

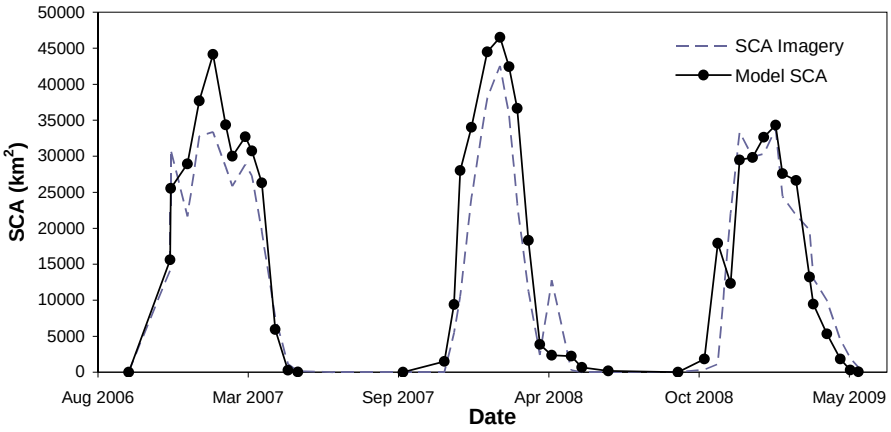

Figure 3-4. Time series comparison of modeled SCA and high-resolution SCA imagery.

A spatial analysis was performed to determine if the location of modeled snow matches the observed snow. The analysis was conducted for each date when SCA images were available. Each pixel within the watershed was classified based on whether the imagery and the model both had snow, both had no snow, or one contained snow but not the other. Any pixels classified as clouds in the SCA image were not included in the analysis. In some cases, there is a blocky effect in the modeled snow covered area caused by the grid size of the TRMM data. This effect disappears as the snowcover reaches its maximum extent.

Figures 3-5, 3-6, and 3-7 show the spatial comparison throughout the 2006–07, 2007–08 and 2008–09 winter seasons, respectively. A visual inspection of the 2006–07 results shows that the model underestimated the snow extent early in the season, and then overestimated it in January. For the remainder of the season, the model and observed SCA compare quite well. In 2007–08 and 2008–09, the opposite occurred; the snow extent was overestimated early and underestimated in the late-spring by the model.

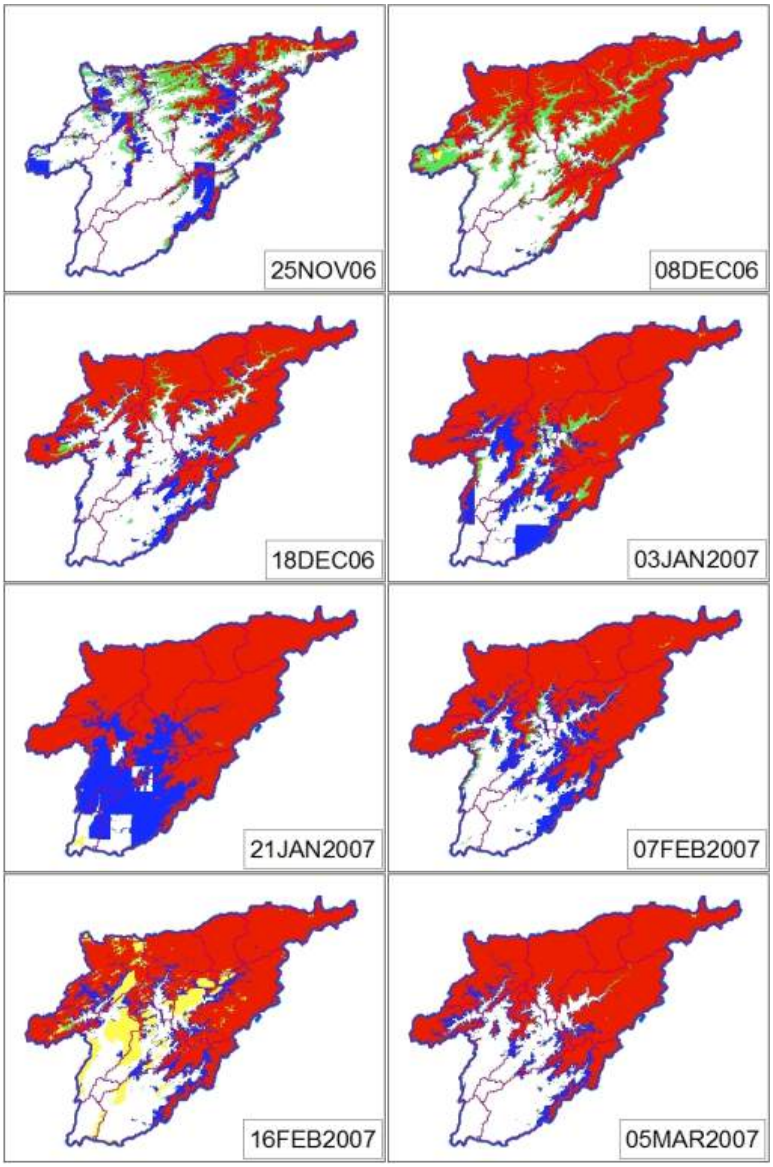

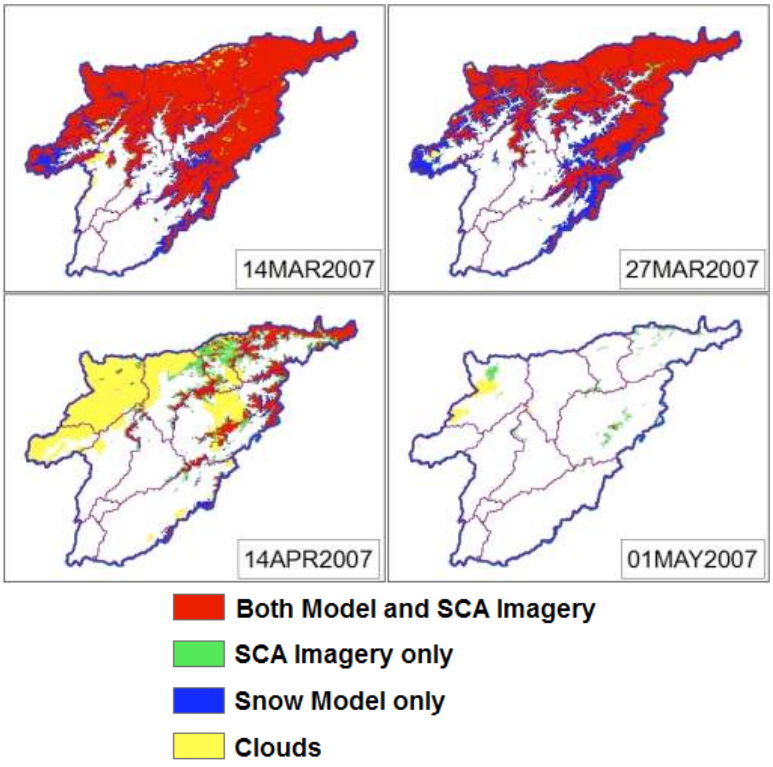

Figure 3-5. SCA comparison during winter 2006–07.

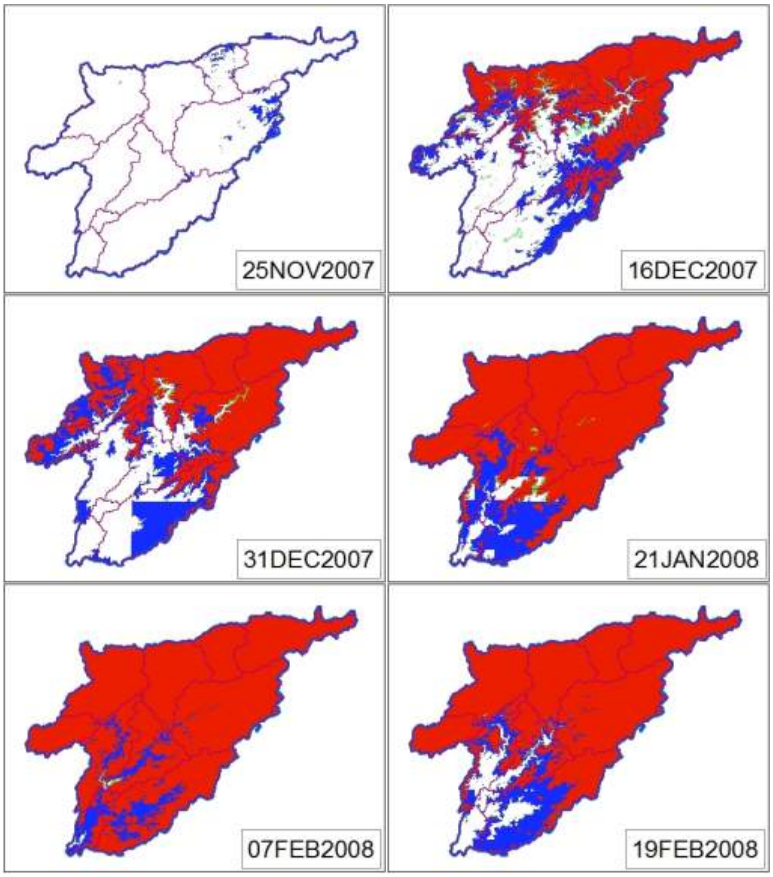

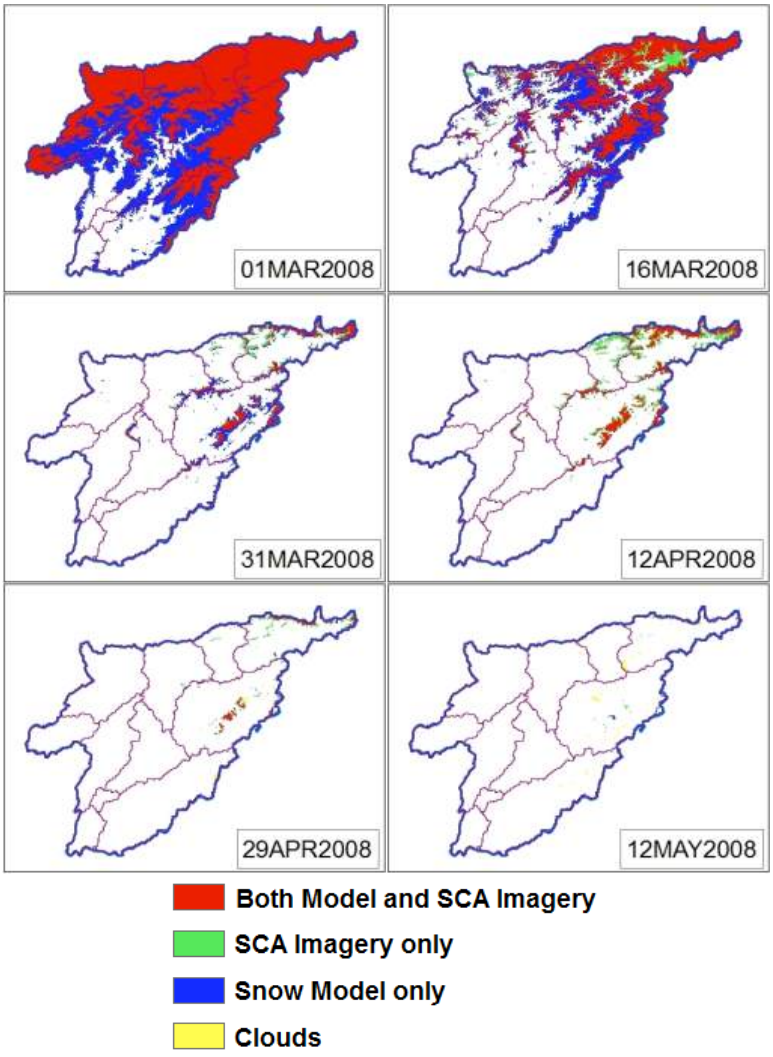

Figure 3-6. SCA comparison during winter 2007–08.

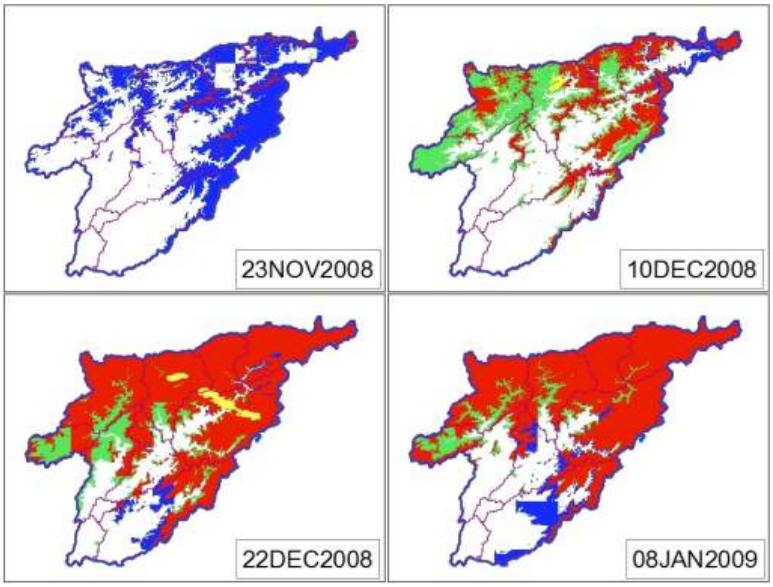

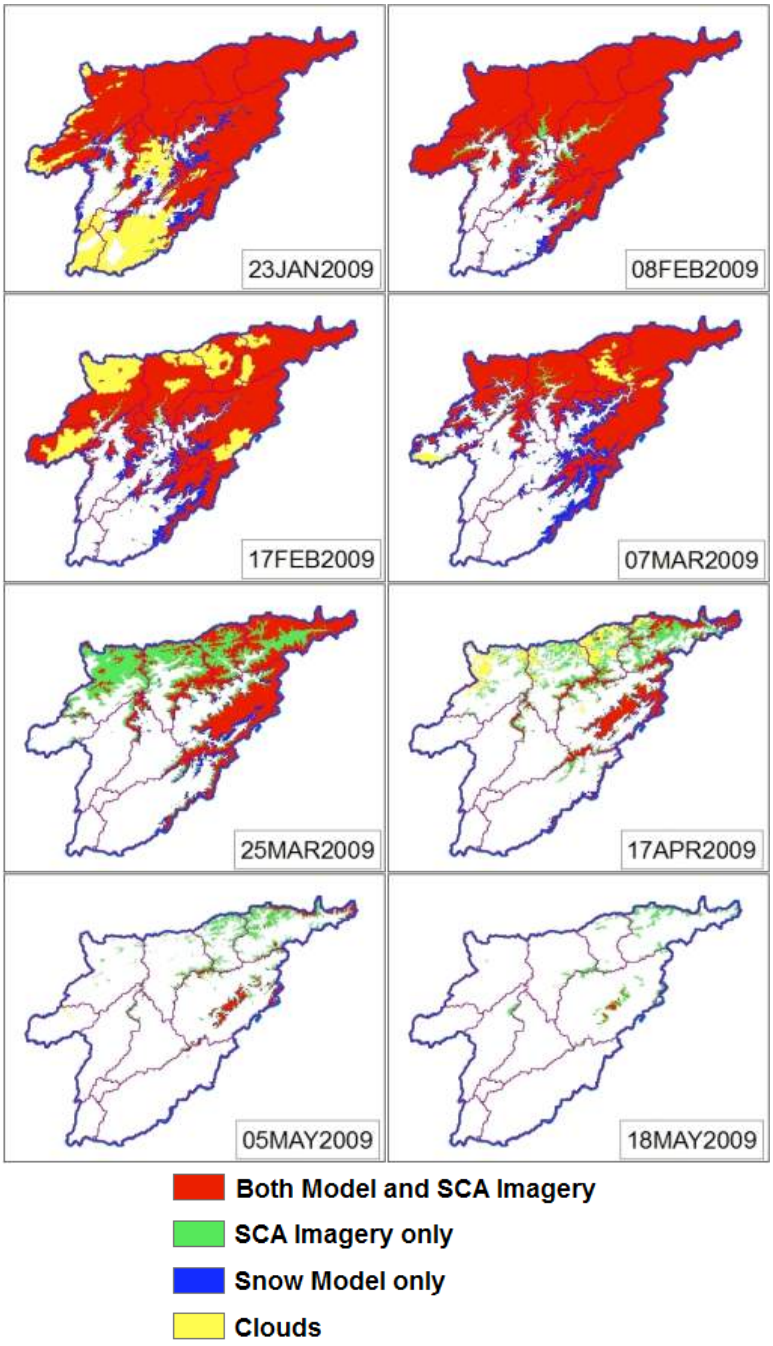

Figure 3-7. SCA comparison during winter 2008–09.

For each comparison an error matrix was computed (Congalton 1991). The overall accuracy is the percentage of pixels that were correctly classified by the model. The overall accuracy ranged from 64.0 to 99.6%, with an average of 87% and a standard deviation of 8.4% (Table 3-4). The user's and producer's accuracies, which describe how well the model did in each category, were also reported. The producer's accuracy is the number of snow (no snow) pixels correctly classified by the model compared to the total

number of snow (no snow) pixels in the reference dataset, and describes how often the model correctly identifies a given type of pixel. The user's accuracy is the number of snow (no snow) pixels correctly classified by the model compared to the total number of snow (no snow) pixels that the model predicted. The user's accuracy describes how reliable the model results are in identifying a given pixel type. A low producer's accuracy means that the model is under-predicting the observations, while a low user's accuracy means the model is over-predicting the observations.

Table 3-4. SCA error matrix accuracy.

2006–07	Overall accuracy (%)	2007–08	Overall accuracy (%)	2008–09	Overall accuracy (%)
25 Nov 2006	83.2	25 Nov 2007	96.8	05 Nov 2008	97.0
08 Dec 2006	85.2	08 Dec 2007	70.8	23 Nov 2008	64.0
18 Dec 2006	87.4	16 Dec 2007	79.1	10 Dec 2008	72.9
03 Jan 2007	84.6	25 Dec 2007	90.4	22 Dec 2008	84.3
21 Jan 2007	77.1	31 Dec 2007	78.2	08 Jan 2009	86.0
07 Feb 2007	85.2	21 Jan 2008	85.1	23 Jan 2009	91.9
16 Feb 2007	89.5	07 Feb 2008	91.4	08 Feb 2009	94.2
05 Mar 2007	91.5	19 Feb 2008	85.7	17 Feb 2009	91.0
14 Mar 2007	91.5	01 Mar 2008	72.0	07 Mar 2009	87.5
27 Mar 2007	83.5	16 Mar 2008	79.5	14 Mar 2009	88.3
14 Apr 2007	88.3	31 Mar 2008	93.9	25 Mar 2009	79.0
01 May 2007	97.5	12 Apr 2008	95.1	30 Mar 2009	82.2
14 May 2007	99.6	16 Apr 2008	77.1	17 Apr 2009	86.4
		29 Apr 2008	98.5	05 May 2009	92.8
		12 May 2008	99.5	18 May 2009	96.2
				29 May 2009	98.6
Average	88.0		86.2		87.0
Std Dev.	6.1		8.8		9.0

In 2006–07, the producer's accuracy for snow-classified pixels is low in the first image and in the last three images, indicating that the model is under-predicting the snow extent at the beginning and end of the winter season, while the mid-winter snow covered area agrees quite well. In 2007–08 the producer's accuracy for snow-classified pixels again indicates that the model is underestimating snow extent at the end of the season, but during the early part of the season the model is overestimating. The 2008–09 SCA comparison gave similar results to 2007–08; the user's accuracy is low for snow-classified pixels in the first two images and low in

producer's accuracy for the last six images, meaning that the model overestimated early in the season and underestimated late in the season. Spatial differences could be caused by incorrectly modeling the precipitation as snow or rain based on the input temperature data, or melting the snow too fast or slow.

Error matrices for all images during each of the three winter seasons, 2006–07, 2007–08 and 2008–09, give overall accuracies of 87.4, 87.0, and 87.0%, respectively (Table 3-5). The overall accuracy of the snow model based on this spatial comparison to the SCA imagery exceeds the 85% accuracy level generally used to evaluate remotely sensed data (Congalton and Green 2009). The producer's accuracies consistently show the model underestimating the snow extent at the end of the season when approximately 25% or less of the basin is snow covered. The model results are quite promising given the scarcity of data in the region. The model is adequately representing snow extent throughout the winter season. An error matrix for each image appears in Appendix B.

Table 3-5. Example SCA error matrix for all images, 2006–07.

		SCA Imagery				
	2006-07	Snow	No Snow		User's accuracy	
HMS Snow Model	Snow	257609	54672	312281	snow	82.5%
	No Snow	19508	256006	275514	no snow	92.9%
		277117	310678	587795	Producer's accuracy	
					snow:	93.0%
		overall accuracy:		87.4%	no snow:	82.4%

3.2.2 SWE Comparison

The total volume of SWE in the Upper Helmand watershed calculated by the model was compared to the AMSR-E estimate of SWE for each winter season (Fig. 3-8). For most years, the timing and magnitude of SWE is similar for both datasets. During two winter seasons, 2003–04 and 2005–06, the model SWE is much lower than the AMSR-E SWE. These 2 years also had lower than normal precipitation based on the TRMM and gage precipitation data. In contrast, the AMSR-E data are relatively consistent year to year. Notably, in the early winter season, AMSR-E frequently detects snow before the model predicts a snowpack. For all years, the AMSR-E and model SWE have a correlation of 0.53 and a Nash-Sutcliffe efficiency measure of 0.2. The RMSE is 18.45 mm with a bias of 7.54 mm. The statistics improve on an annual basis if the 2 years with large discrepancies are removed, with efficiencies ranging from 0.2–0.8 (Table 3-6).

Table 3-6. Evaluation statistics comparing AMSR-E SWE to snow model results, entire basin.

	2003–04	2004–05	2005–06	2006–07	2007–08	2008–09	All Years
Correlation	0.81	0.64	0.54	0.51	0.78	0.70	0.5
Nash-Sutcliffe	–13.1	0.5	–12.1	0.2	0.8	0.5	0.2
RMSE (mm)	23.8	13.4	22.3	20.5	15.3	12.4	18.5
Bias (mm) AMSR-E - Model	15.2	3.5	15.0	6.0	1.1	4.8	7.5

A spatial comparison of model and AMSR-E SWE was conducted monthly each winter. Model SWE grids were selected on a day in the middle of each month when no AMSR-E data were missing, and aggregated to match the 25-km^2 AMSR-E grids. Figure 3-9 shows a series of monthly comparisons made during the 2006–07 winter season. The model and AMSR-E estimates of SWE agree better where the snowpack is thinner, in the beginning and end of the winter season, and at the lower elevations. In midwinter, the AMSR-E detects more SWE than the model at the higher elevations, subbasins 1–4, while the model SWE values are consistently greater in the southern region of the watershed, subbasin 9. Other years produced similar patterns (Appendix C). The difference between AMSR-E and model SWE at the higher elevations is largest in March 2006. In January and February 2008, the model predicted more SWE than the AMSR-E throughout much of the watershed. This reversed in March 2008, when the model and AMSR-E SWE agree at the lower elevations and the AMSR-E is greater at the higher elevations. This corresponds with the time series of SWE.

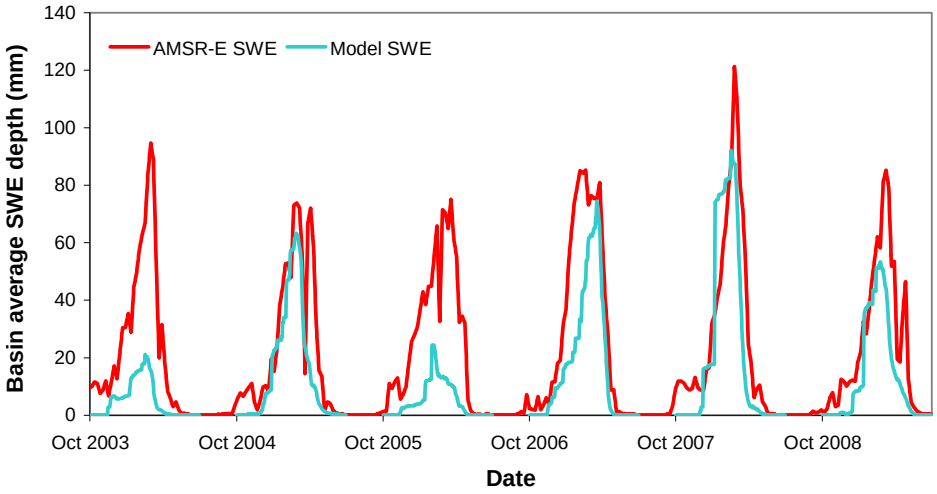

Figure 3-8. Comparison of modeled and AMSR-E SWE depth in Upper Helmand Watershed.

The difference in SWE in the southern region was unexpected. Possible reasons for this difference include: precipitation is modeled as snow because of lower than actual temperatures in this area; the TRMM data are overestimating precipitation in this region; or the AMSR-E sensor is not detecting the snow in this region, possibly because of the north-facing slope orientation. In the SCA analysis, this region tended to be overestimated by the model, and the estimated precipitation in subbasin 9 was not significantly different from the other subbasins, which supports the idea that low interpolated temperatures are the cause.

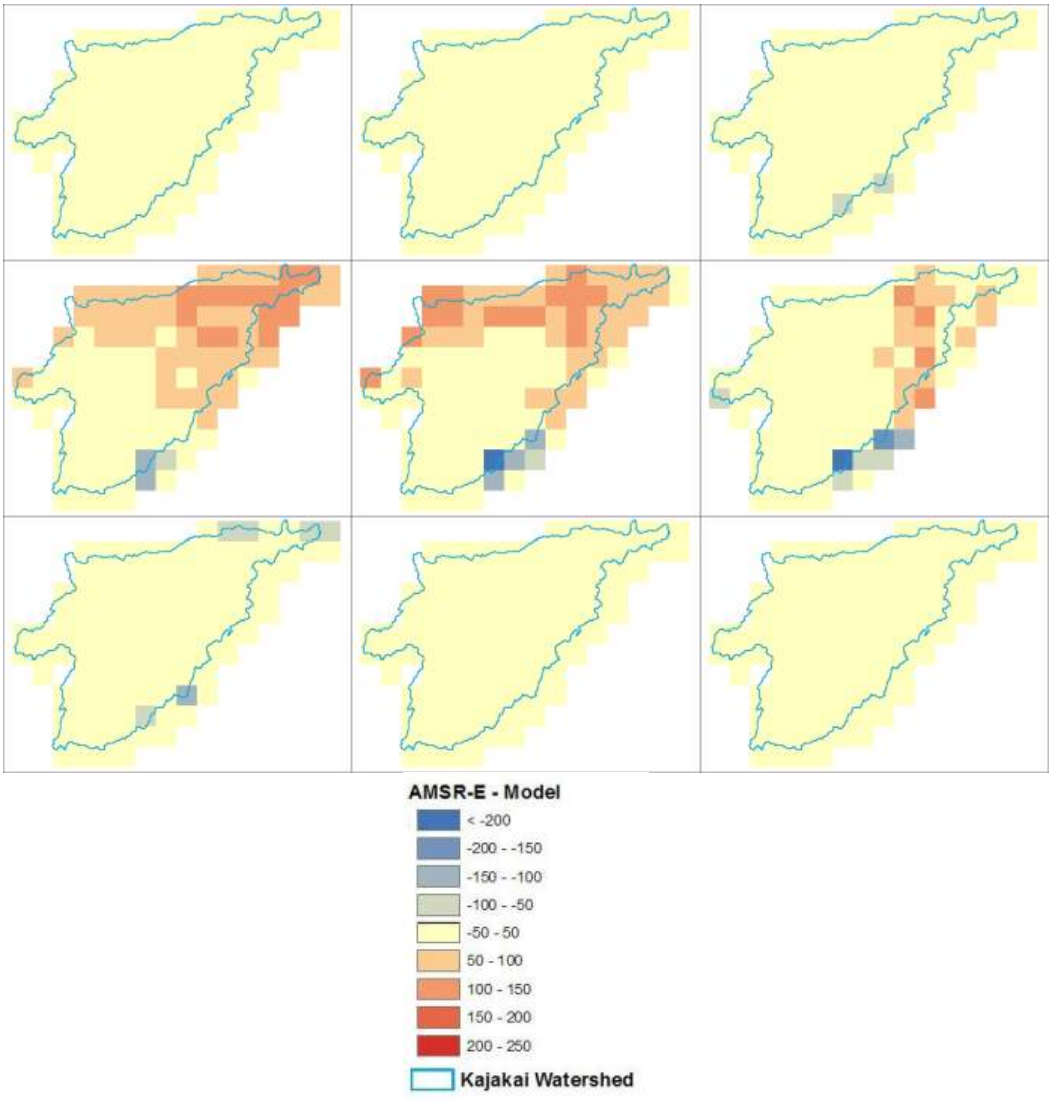

Figure 3-9. Example spatial comparison of AMSR-E and modeled SWE for 2006–07.

An error matrix, similar to that used in the SCA comparison, was computed for each monthly comparison by classifying each pixel into 50-mm

bins (Table 3-7). An overall match was computed by calculating the percentage of pixels that agree between the two datasets (Table 3-8). In the early and late winter seasons, both model and AMSR-E SWE values are small and the overall matches are high, near 100%. In mid-winter, the SWE values do not agree as well; the average monthly overall match for January–March ranges between 55–62%. The date on which the comparison was made can affect the results of the error matrix analysis; however, effort was made to select dates when AMSR-E data were not affected by wet snow.

Table 3-7. Example SWE error matrix for all months 2006–07.

		Model SWE (mm)						
		0-50	50-100	100-150	150-200	200-250	250-300	
AMSR-E SWE (mm)	0-50	540	13	1	1	2	0	557
	50-100	36	9	7	0	1	0	53
	100-150	31	27	10	0	0	1	69
	150-200	2	20	1	0	0	0	23
	200-250	0	0	0	0	0	0	0
	250-300	0	0	0	0	0	0	0
		609	69	19	1	3	1	702
							Overall match:	79.6%

Table 3-8. SWE error matrix overall match (%).

Year	Oct	Nov	Dec	Jan	Feb	Mar	Apr	May	Jun	Total Season
2003–04	100	100	86	92	51	82	100	100	100	90
2004–05	100	100	97	58	55	72	72	99	100	84
2005–06	100	100	77	73	91	46	69	100	100	84
2006–07	100	100	92	38	38	54	94	100	100	80
2007–08	100	100	99	24	38	62	96	100	100	80
2008–09	100	100	100	63	59	54	64	99	100	82

3.3 Hydrologic model results

The HMS model was calibrated to the 2006–07 winter season when daily reservoir water level data were available (Fig. 3-10). Particular emphasis was placed on matching the peak flows, given that the reservoir elevation–discharge relationship is less reliable for smaller inflows. Two peaks

occurred in the model runoff during in late March and early April of 2007, which correspond to the observed peak inflows. While the first peak is higher in the model than in the observed inflow, the timing and magnitude of the second peak matches on the same day and is within 2% of the observed. The magnitude of each of the model peaks represents a significant flow event compared to the historical streamflow records. According to the Dartmouth Flood Observatory archives (2008), major flooding affected much of Afghanistan between 18 March and 5 April 2007 caused by rain and snowmelt. In the Helmand Province, the record states, "hundreds were evacuated" and "dams on the Helmand River were close to maximum capacity" thus supporting the model results.

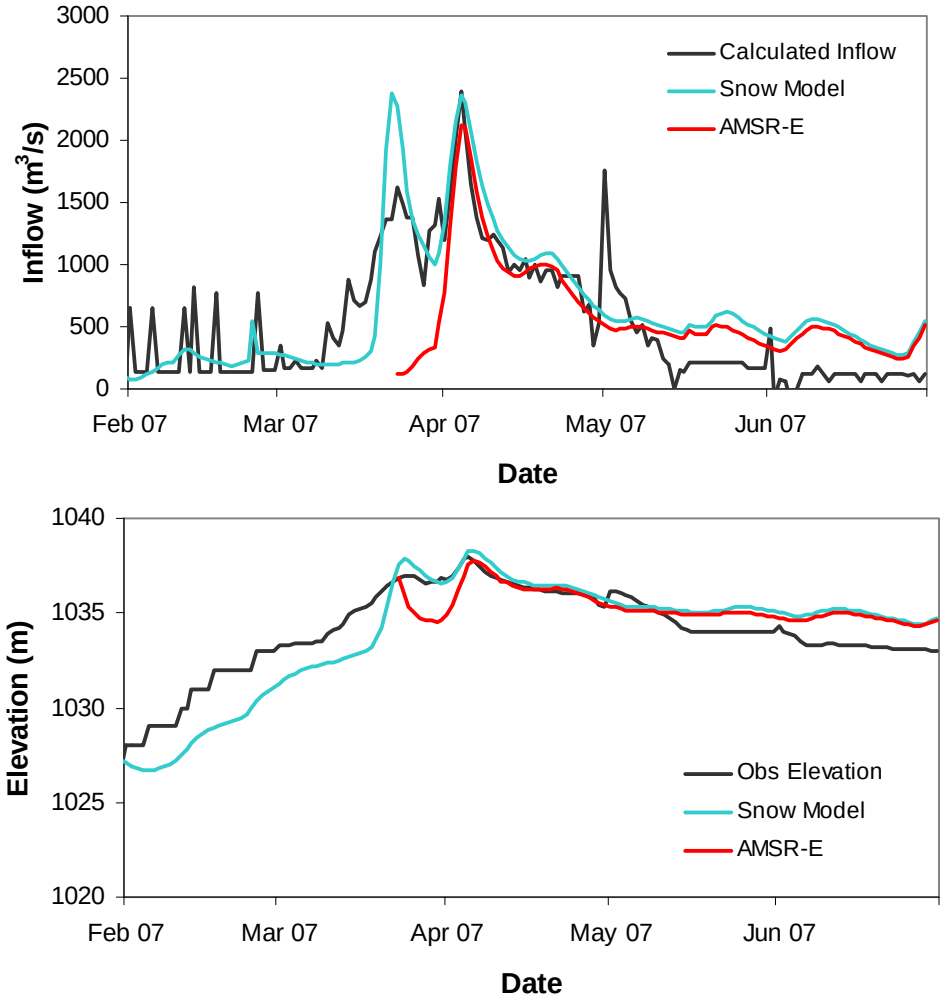

Figure 3-10. Comparison of daily reservoir inflows and water surface elevation for 2007; observed data (black), HMS snow model results (green), and model results using initial AMSR-E SWE (red).

Once the model was calibrated to the 2006–07 winter season, it was run over the remaining five winter seasons, starting in October and ending in June, to capture the entire snow accumulation and melt period. Next, the model was initialized using AMSR-E SWE grids at the date of the approximate maximum SWE for each of the 6 years. Statistics are calculated to compare the model results, with and without initial AMSR-E SWE, to observations during the time periods each year when all data are available (Table 3-9).

Table 3-9. Model evaluation statistics for time periods when AMSR-E model results are available.

	Observed	HMS model	HMS model with AMSR-E initial SWE
Daily inflow			
Average (m^3/s)	519.1	543.9	458.8
Standard deviation (m^3/s)	471.9	441.5	341.0
Bias (m^3/s)		24.8	–60.3
RMSE (m^3/s)		304.3	357.4
Correlation		0.61	0.44
Nash-Sutcliffe efficiency		0.57	0.42
Daily stage			
Average (m)	1034.9	1035.1	1034.8
Standard deviation (m)	1.3	1.1	1.1
Bias (m)		0.2	–0.1
RMSE (m)		0.9	0.9
Correlation		0.50	0.51
Nash-Sutcliffe efficiency		0.43	0.48
Monthly stage			
Average (m)	1032.1	1029.7	1032.4
Standard deviation (m)	2.9	6.8	2.9
Bias (m)		–2.5	0.3
RMSE (m)		5.9	1.2
Correlation		0.40	0.83
Nash-Sutcliffe efficiency		–3.35	0.81

3.3.1 HMS model results

Observed daily inflows and water surface elevations were compared to model results in 2009 (Fig. 3-11). During the spring of 2009, the model

underestimates water levels and inflows during the spring runoff, though the timing matches. The correlations for the daily inflow and stage are 0.6 and 0.5, respectively. The Nash-Sutcliffe efficiency between the modeled and observed daily inflow is 0.57, and between the modeled and observed stage is 0.43. For the remaining four winter seasons, modeled reservoir elevations were averaged monthly for comparison to observed monthly elevations (Fig. 3-12). In 2003–04 and 2005–06, the model significantly underestimates the reservoir stage. During the remaining 4 years, the peak water levels calculated by the model match the observed reasonably well. However, owing to the 2 low years, the overall correlation is reduced to 0.4 and the Nash-Sutcliffe efficiency to –3.35. Because estimating the total water supply is a primary objective of this study, the water balance of the reservoir was examined (Table 3-10). In 2003–04 and 2005–06, a net decrease in storage was predicted when in fact there was a gain. All other years do reasonably well matching the observed data and overall change in storage. The average monthly storage, modeled and observed, for all years has a correlation of 0.61 (Fig. 3-13).

Table 3-10. Kajakai Reservoir water balance, HMS results and observed change in storage.

Model Results	2003–04	2004–05	2005–06	2006–07	2007–08	2008–09
Total volume inflow (10^7 m^3)	269	577	209	987	418	467
Total outflow (10^7 m^3)	296	508	218	927	399	397
Change in storage (10^7 m^3)	–28	69	–9	60	19	70
Date of peak stage	3 Mar 04	23 Mar 05	3 May 06	5 Apr 07	16 Mar 08	16 Apr 09
Peak stage (m)	1031.4	1036.5	1023.0	1038.3	1034.7	1035.6
Observed						
Change in storage (10^7 m^3)	1	64	56	66	25	68

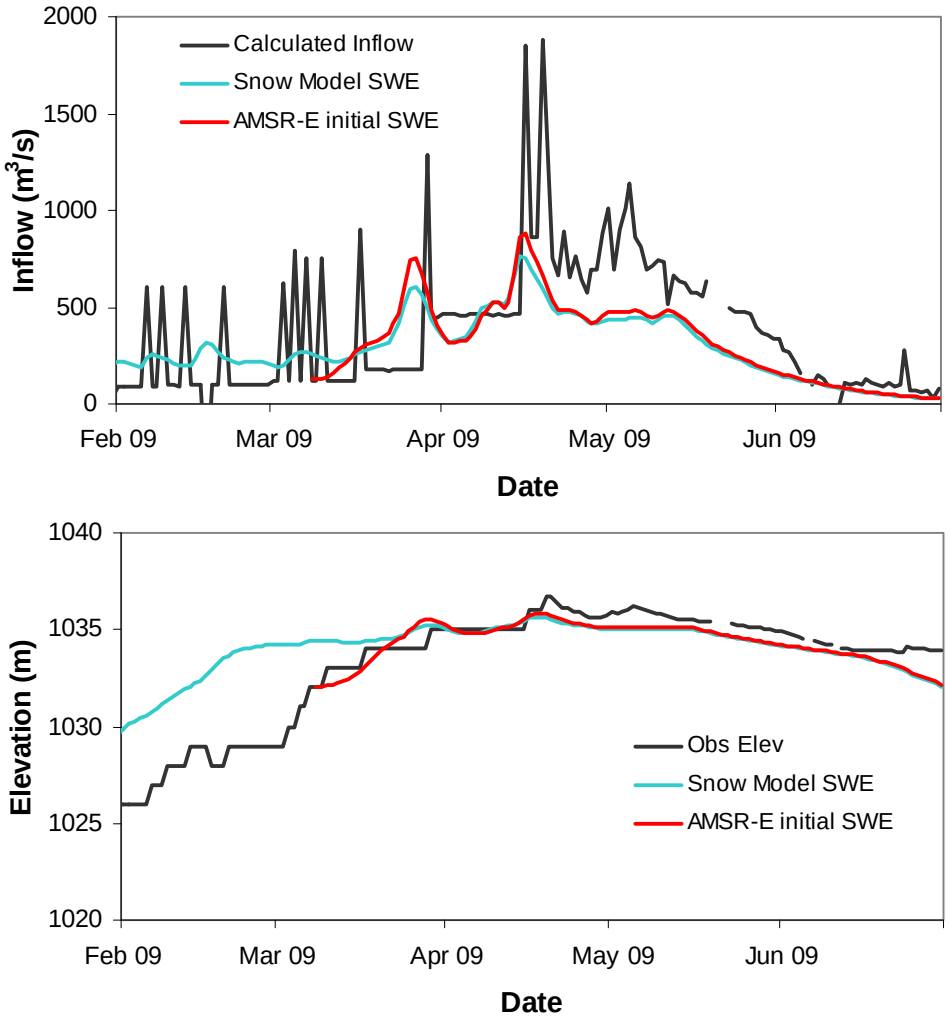

Figure 3-11. Comparison of daily reservoir inflows and water surface elevation for 2009; observed data (black), HMS snow model results (green), and model results using initial AMSR-E SWE (red).

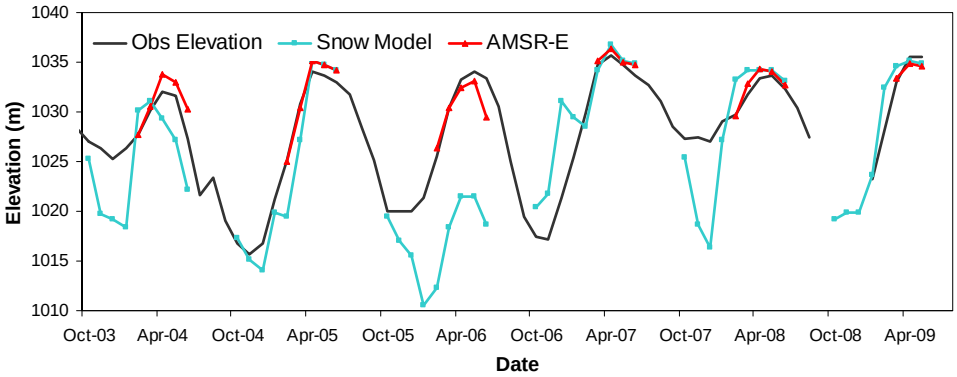

Figure 3-12. Comparison of monthly reservoir water surface elevations for water years 2004–2009; observed data (black), HMS snow model results (green), and model results using initial AMSR-E SWE (red).

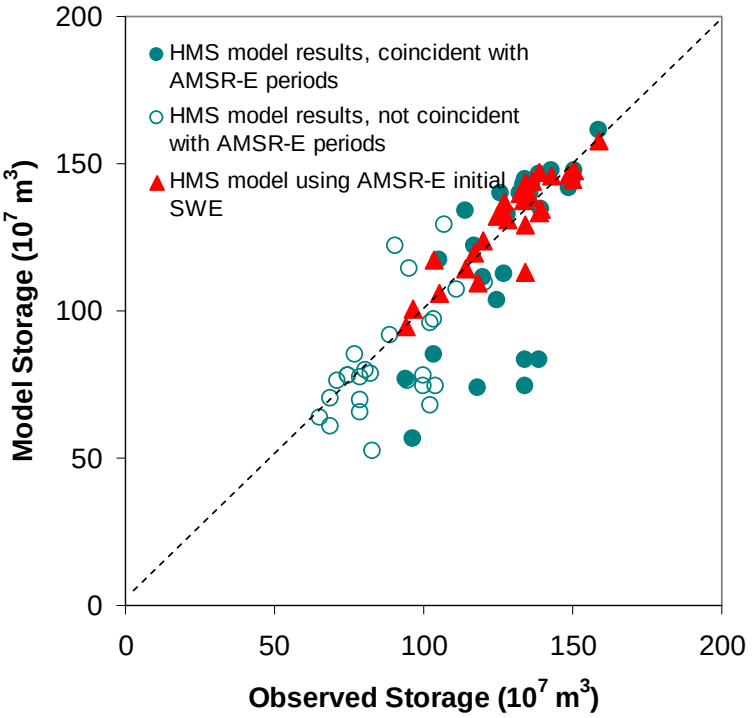

Figure 3-13. Comparison of observed average monthly storage in the Kajakai Reservoir with entire winter model results and AMSR-E initial SWE model results.

3.3.2 AMSR-E initial SWE

The model was run using AMSR-E SWE data to evaluate how well the spring reservoir inflows and stage could be predicted if initialized with passive microwave snow data. The starting dates were determined by analyzing the model and passive microwave SWE and selecting the date when the SWE reached an approximate maximum. This minimizes the amount of additional snow accumulation and focuses the analysis on the volume of SWE estimated by AMSR-E.

The model results using initial AMSR-E SWE grids are shown with the HMS model results for the entire winter season (Fig. 3-10, 3-11 and 3-12), and compared statistically in Table 3-8. Using the AMSR-E SWE as initial conditions produced similar daily runoff and stage results in 2006–07 and 2008–09 as the model results without the initial SWE. The correlations for the daily inflow and stage are 0.4 and 0.5, respectively. The Nash-Sutcliffe efficiency between the modeled and observed daily inflow is 0.42, and between the modeled and observed stage is 0.48.

The monthly results greatly improved using AMSR-E SWE to initialize the model, particularly in 2003–04 and 2005–06, when the original water levels were much lower than the observed. For all years, the correlation between the average monthly water levels using AMSR-E SWE and observed is 0.83, and the Nash-Sutcliffe efficiency is 0.81. This is a significant improvement over the model results that did not use the initial AMSR-E SWE, which had a correlation of 0.40 over the same time period.

3.3.3 Passive microwave signal observations

Typically, the estimated SWE from passive microwave steadily rises during the accumulation period, and then becomes increasingly scattered in the spring when the snow saturates because of melt or rainfall. Occasionally, the basin average SWE will rapidly decrease to near zero, then return to approximately the original value over several days. This occurrence is visible even in the weekly maximum SWE data (Fig. 3-3). This likely occurs because wet snow can cause the remotely sensed SWE to decrease. The passive microwave signal does not scatter through water so the difference in temperature brightness at two different frequencies becomes minimal, thus reducing the estimate of SWE.

During the study period, a number of rapid decreases in SWE were observed. Analysis indicates that they typically occurred during or shortly after a precipitation event and supports the theory that they are caused by wet snow. The time series of AMSR-E SWE was compared to modeled reservoir inflows (2004–2009) and observed daily inflows (2007 and 2009). For each decrease that was noted in the AMSR-E data, a notable increase in the modeled inflow was observed (Table 3-11). The typical time lag between the AMSR-E anomaly and the inflow increase was 4 days, which is a reasonable travel time for the rainfall and snowmelt to reach the reservoir given the hydrological analysis of the time of concentration (0.5–1 day) and routing times (1.5 days per reach). In 2007, there was a 6-day time lag between the SWE decrease on 16 March and the inflow increase on 22 March. The snowpack was deeper during this event than any other when a decrease was noted and it is possible that this caused a delay in the runoff. Another explanation could be that the precipitation event was stationary over the region for a longer period

Table 3-11. Significant AMSR-E SWE decreases and inflow increases.

Date of AMSR-E minimum	Decrease in basin-average AMSR-E SWE (mm)	Date of inflow peak	Discharge increase between dates (m^3/s)
11 Jan 04	21	15 Jan 04	245.5
15 Mar 05	52	19 Mar 05	1736.3
16 Mar 07	74	22 Mar 07	2132.2
30 Mar 07	73	3 Apr 07	1275.9
22 Mar 09	50	26 Mar 09	249.45

4 Discussion

4.1 Precipitation results

Accurate observations of precipitation are critical for hydrologic modeling success. Several studies have investigated the accuracy of satellite precipitation measurements for use in hydrologic applications (Hossain and Anagnostou 2006; Hossain and Huffman 2008; Rahman et al. 2009) to develop a standard approach for reporting error. The volume of precipitation is important, as are the temporal and spatial distribution of the data. Estimating the error in the measurements is difficult given the large pixel size of the satellite data. Finding appropriate methods of comparison between different scales (e.g., point measurements and satellite data) is an important area of investigation given the increasing use of remotely sensed data.

Model results were affected by low precipitation during the 2003–04 and 2005–06 winter seasons when annual precipitation was below normal. This was evident in the hydrologic model results, and supported in the comparison of snow model results to passive microwave SWE. Additionally, the low model SWE in the higher elevations as compared spatially to passive microwave SWE may indicate a consistent underestimation of precipitation by TRMM. Several studies have adjusted satellite estimates of precipitation to improve hydrologic model results by applying a local bias correction (Harris et al. 2007; Stisen and Sandholt 2010) or using a linear regression (Immerzeel and Droogers 2008) with station observations. Future hydrologic studies of Afghanistan should consider applying similar techniques by analyzing the gage precipitation with TRMM data. Additional meteorological stations and a better understanding of orographic effects in this region will improve precipitation estimates and model results.

4.2 Snow model results

High-resolution SCA images provided a good calibration tool for the snow model. In general, the modeled snow extent matched the SCA imagery throughout the winter season. Other studies have similarly used SCA imagery as a calibration tool with good results (Parajka and Bloschl 2008; Kuchment et al. 2010). Further SCA comparison during the 2003–04 and

2005–06 winter seasons, when precipitation estimates were low, would help to determine if SCA imagery could be used to identify periods in which snow extent is underestimated. The snow model was most sensitive to the temperature lapse rate used to develop the interpolated daily temperature grids. A switch from using a typical lapse rate to a regional lapse rate calculated using gage measurements improved model results considerably. Other snow model parameters were less sensitive.

Studies assessing the accuracy of passive microwave SWE using point ground measurements have seen a variety of results. Mote et al. (2003) compared observed snow depths in the U.S. Midwest to SSM/I SWE and found generally good agreement, with differences ranging from 2–22 mm. Derksen et al. (2003) analyzed 18 years of passive microwave data over Canada and found that performance was strongly linked to land cover, with estimates in open areas showing strong agreement. In contrast, Tekeli (2008) compared ground measurements to passive microwave estimates of SWE in the mountainous regions of Turkey and found differences ranging from –218 to +93 mm. However, Chang et al. (2005) suggest that at least 10 stations are needed within a $1 \times 1°$ area to accurately compare point measurements to the large passive microwave pixel area. This sort of ground coverage is difficult to obtain without a dedicated field campaign and unlikely to occur in data-scarce countries.

The comparison of model SWE to passive microwave SWE in the Upper Helmand watershed demonstrates that both estimates give a similar magnitude of snow mass in most years. The timing of snow accumulation and melt agree quite well in some periods and less so in others. In 2003–04 and 2005–06, the model estimates are much lower than the passive microwave data. Without ground measurements it is impossible to say which is closer to the true value of SWE, though hydrologic modeling results suggest that the model is affected by poor precipitation data during the low SWE years.

4.3 Hydrologic results

The HMS model of the Upper Helmand watershed was used to model the hydrologic conditions of the basin and simulate inflows to the Kajakai Reservoir. Results of a water balance analysis agree with limited observations and provide practical information about the snow and streamflow characteristics. The need for ground-based meteorological and hydrological observations in Afghanistan is well understood. Each year, additional sta-

tions are installed where possible. Longer, distributed data observations will help improve model results. While precipitation data influenced the estimated volume of water, the model timing and peak flows were also sensitive to infiltration parameters. A better understanding of the groundwater processes in this region would improve model results, as would discharge measurements upstream of the reservoir. The use of passive microwave observations to initialize the model removed some of the uncertainty in the precipitation estimates. Future investigations to increase capacity or forecast inflows to the Kajakai Reservoir should consider this approach.

Several studies have tried to correlate satellite estimates of SWE to stream runoff with mixed results. A correlation analysis between remotely sensed SWE and streamflow data from three major Siberian watersheds (Yang et al. 2007) and in the Yukon River basin (Yang et al. 2009) found statistically significant relationships between the data. Rawlins et al. (2007) compared mid-winter SWE from SSM/I to total spring runoff in 179 arctic basins and found poor and even negative correlations. This was attributed to vegetation effects in some regions and saturation of the passive microwave signal. Andreadis and Lettenmaier (2006) assimilated passive microwave SWE into a hydrologic model of the Snake River basin in the western U.S. They found that passive microwave data only improved model results for shallow snowpacks, and introduced error when a snowpack deeper than 240 mm was present, again attributed to saturation of the signal. In contrast, Wilson et al. (1999) developed a distributed snow hydrology model of the Rio Grande River in Colorado, and used SSM/I SWE to periodically update the snow parameters through inversion. They found that modeled SWE better matched observed data when updated with passive microwave data. In the Upper Helmand watershed, error in the passive microwave signal caused by vegetation or saturation limit is likely minimal, given that there is little vegetation and the snow does not reach significant depths. However, topography may still be a concern. Given the resolution of the passive microwave data, the large size of the watershed may average out some of the local data uncertainty.

The sensitivity of the passive microwave data to wet snow is just beginning to be seen as a potential source of valuable hydrologic information, and no studies were found that used this information to predict runoff. This study found that periods when the signal is impacted consistently correspond to increased flows into the reservoir following a rapid decrease in the SWE

time series. Further investigations are needed to understand the physical processes causing these anomalies and their potential value to runoff predictions.

5 Conclusions

A snow hydrology model of the Upper Helmand watershed in Afghanistan was developed to increase our understanding of the water processes in this data-scarce region. This research focused on characterizing the snowpack in this remote, mountainous region to compare model results to remotely sensed SWE. The model used TRMM precipitation and interpolated gage temperature data as input and calculated SWE using a temperature index method. The snow model was calibrated to high-resolution SCA imagery, and was able to accurately simulate the snow accumulation and melt process. The hydrologic model was calibrated to observed data at the Kajakai Reservoir. The model was able to reasonably simulate inflows to the reservoir and the volume of water stored in the basin. This improves our understanding of the hydrologic processes in this region. In particular, the snow extent and mass are better quantified as well as the contribution of snow to runoff.

Improvements to the precipitation estimates, including bias correction of the satellite data, additional ground-based meteorological stations, and a better understanding of the distribution of precipitation in this region, will improve model results. Model calibration was particularly sensitive to infiltration parameters. Future investigations of the soil characteristics in this region would lead to a better estimation of losses. Discharge measurements will provide further validation to the model and increase our understanding of the hydrology in this basin.

This study found that passive microwave SWE provides reasonable estimates of the snow mass and its distribution in the Upper Helmand watershed. Without ground based snow measurements, passive microwave data can provide important information to water resource managers and reservoir operators. Additionally, using passive microwave SWE to initialize hydrological models adds value to water supply planning and dam management. Passive microwave SWE also has potential use in forecasting reservoir inflows, both in conjunction with the hydrologic model, and by analyzing the strong response to wet snow. In this data-scarce region of central Afghanistan, passive microwave SWE provides valuable water resource information.

References

AIMS. 1997. *Afghanistan Shapefiles*. Afghanistan Information Management Service (AIMS), Islamabad, Pakistan.

Anderson, E. 2006. *Snow accumulation and ablation model—SNOW-17.* National Weather Service River Forecast System User Manual. NOAA.

Andreadis, K. M., and D. P. Lettenmaier. 2006. Assimilating remotely sensed snow observations into a macroscale hydrology model. *Advances in Water Resources* 29: 872–886.

Armstrong, R. L., and M. J. Brodzik. 1995. An earth-gridded SSM/I data set for cryospheric studies and global change monitoring. *Advances in Space Research* 16: 155–163.

Barnett, T. P., J. C. Adam, and D. P. Lettenmaier. 2005. Potential impacts of a warming climate on water availability in snow-dominated regions. *Nature* 438: 303–309.

Blue, A. C. 2006. *Kajakai Dam inundation study, Kajakai Dam and Reservoir, Helmand Province, Afghanistan*. U.S. Army Corps of Engineers.

Burger, A. S. 2005. *Calibration of a precipitation runoff model for the Hirmand River in Afghanistan and Iran using remote sensing data*. Masters. Delft University of Technology, Delft, The Netherlands.

Chang, A. T. C., R. E. J. Kelly, E. G. Josberger, R. L. Armstrong, J. L. Foster, and N. M. Mognard. 2005. Analysis of ground-measured and passive-microwave-derived snow depth variations in midwinter across the northern Great Plains. *Journal of Hydrometeorology* 6: 20–33.

Chirico, P., and M. Warner. 2005. *Mosaic of digital raster Soviet 1:200,000 - scale topographic maps of Afghanistan*. U.S.Geological Survey.

Congalton, R. G. 1991. A review of assessing the accuracy of classifications of remotely sensed data. *Remote Sensing of Environment* 37: 35–46.

Congalton, R. G., and K. Green. 2009. *Assessing the accuracy of remotely sensed data: principals and practices*, Second edition. CRC Press, Taylor & Francis Group.

Cosgrove, W. J., and F. R. Rijsberman. 2000. *World water vision: Making water everybody's business*. Earthscan Publications, London.

Daly, S. F., J. Hardy, E. Ochs, S. Newman, T. Baldwin, C. Vuyovich, J. Gagnon, and B. Tracy. 2004–2010. *Assessment of the state of the snowpacks in the major Afghanistan snow-impacted watersheds*. A series of bi-weekly assessments prepared between December and May for the US Army, and the US Army Corps of Engineers. ERDC-CRREL.

Daly, S. F., E. Ochs, P. Brooks, T. Pangburn, and E. Davis. 1999. Distributed snow process model for use with HEC-HMS. *Cold Regions Engineering: Putting Research into Practice.* ASCE, Lincoln, NH.

Derksen, C., A. Walker, and B. Goodison. 2003. A comparison of 18 winter seasons of in situ and passive microwave-derived snow water equivalent estimates in Western Canada. *Remote Sensing of Environment* 88: 271–282.

Derksen, C., A. E. Walker, B. E. Goodison, and J. W. Strapp. 2005. Integrating in situ and multiscale passive microwave data for estimation of subgrid scale snow water equivalent distribution and variability. *IEEE Transactions on Geoscience and Remote Sensing* 43: 960–972.

DeWalle, D. R., and A. Rango. 2008. *Principles of snow hydrology*, 1st edition. Cambridge University Press.

Favre, R., and G. M. Kamal. 2004. *Watershed atlas of Afghanistan: Working document for planners*, 1st Edition. Food and Agriculture Organization of the United Nations (FAO)

Afghanistan Information Management Service (AIMS), Kabul, Afghanistan.

Foster, J. L., D. K. Hall, A. T. C. Chang, A. Rango, W. Wergin, and E. Erbe. 1999. Effects of snow crystal shape on the scattering of passive microwave radiation. *IEEE Transactions on Geoscience and Remote Sensing* 37: 1165–1168.

Foster, J. L., C. J. Sun, J. P. Walker, R. Kelly, A. Chang, J. R. Dong, and H. Powell. 2005. Quantifying the uncertainty in passive microwave snow water equivalent observations. *Remote Sensing of Environment* 94: 187–203.

Frankenstein, S., A. Sawyer, and J. Koeberle. 2008. Comparison of FASST and SNTHERM in three snow accumulation regimes. *Journal of Hydrometeorology* 9: 1443–1463.

Franz, K. J., T. S. Hogue, and S. Sorooshian. 2008. Operational snow modeling: Addressing the challenges of an energy balance model for National Weather Service forecasts. *Journal of Hydrology* 360: 48–66.

Gafurov, A., and A. Bardossy. 2009. Cloud removal methodology from MODIS snow cover product. *Hydrology and Earth System Sciences* 13: 1361–1373.

Hall, D. K., A. T. C. Chang, and J. L. Foster. 1986. Detection of the depth-hoar layer in the snow-pack of the Arctic Coastal-Plain of Alaska, USA, using satellite data. *Journal of Glaciology* 32: 87–94.

Hallikainen, M. T., F. T. Ulaby, and M. Abdelrazik. 1986. Dielectric-properties of snow in the 3 to 37 ghz range. *IEEE Transactions on Antennas and Propagation* 34: 1329–1340.

Harris, A., S. Rahman, F. Hossain, L. Yarborough, A. C. Bagtzoglou, and G. Easson. 2007. Satellite-based flood modeling using TRMM-based rainfall products. *Sensors* 7: 3416–3427.

Harza. 1976. Kajakai Gates Project, probable maximum flood.*Civil design memorandum C-1 912C*. Harza Overseas Engineering Company, Chicago, IL.

Hock, R. 2003. Temperature index melt modeling in mountain areas. *Journal of Hydrology* 282: 104–115.

Hossain, F., and E. N. Anagnostou. 2006. A two-dimensional satellite rainfall error model. *IEEE Transactions on Geoscience and Remote Sensing* 44: 1511–1522.

Hossain, F., and G. J. Huffman. 2008. Investigating error metrics for satellite rainfall data at hydrologically relevant scales. *Journal of Hydrometeorology* 9: 563–575.

Huffman, G. J., R. F. Adler, D. T. Bolvin, G. J. Gu, E. J. Nelkin, K. P. Bowman, Y. Hong, E. F. Stocker, and D. B. Wolff. 2007. The TRMM multisatellite precipitation analysis (TMPA): Quasi-global, multiyear, combined-sensor precipitation estimates at fine scales. *Journal of Hydrometeorology* 8: 38–55.

Immerzeel, W. W., and P. Droogers. 2008. Calibration of a distributed hydrological model based on satellite evapotranspiration. *Journal of Hydrology* 349: 411–424.

Immerzeel, W. W., P. Droogers, S. M. de Jong, and M. F. P. Bierkens. 2009. Large-scale monitoring of snow cover and runoff simulation in Himalayan river basins using remote sensing. *Remote Sensing of Environment* 113: 40–49.

Jordan, R. 1991. *One-dimensional temperature model for a snow cover; technical documentation for SNTHERM.89*. U.S. Army Cold Regions Research and Engineering Laboratory, Special Report SR 91-16.

Josberger, E. G., and N. M. Mognard. 2002. A passive microwave snow depth algorithm with a proxy for snow metamorphism. *Hydrological Processes* 16: 1557–1568.

Kelly, R., E.J. Alfred, T.C. Chang, J.L. Foster, M. Tedesco. 2004. *AMSR-E/Aqua daily L3 Global snow water equivalent EASE-E Grids*, V002. National Snow and Ice Data Center, Boulder, CO USA.

Kelly, R. E., A. T. Chang, L. Tsang, and J. L. Foster. 2003. A prototype AMSR-E global snow area and snow depth algorithm. *IEEE Transactions on Geoscience and Remote Sensing* 41: 230–242.

Kirpich, Z. P. 1940. Time of concentration of small agricultural watersheds. *Civil Engineering* 10: 362.

Kuchment, L. S., P. Romanov, A. N. Gelfan, and V. N. Demidov. 2010. Use of satellite-derived data for characterization of snow cover and simulation of snowmelt runoff through a distributed physically based model of runoff generation. *Hydrology and Earth System Sciences* 14: 339–350.

Li, X. G., and M. W. Williams. 2008. Snowmelt runoff modeling in an arid mountain watershed, Tarim Basin, China. *Hydrological Processes* 22: 3931–3940.

Maidment, D. R. 1993. *Handbook of hydrology*. McGraw-Hill, Inc.

Marks, D., J. Domingo, D. Susong, T. Link, and D. Garen. 1999. A spatially distributed energy balance snowmelt model for application in mountain basins. *Hydrological Processes* 13: 1935–1959.

Martinec, J., A. Rango, and R. Roberts. 2008. *Snowmelt Runoff Model (SRM) user's manual. WSRM*, Version 1.11. New Mexico State University, Las Cruces, NM.

Matzler, C., and A. Standley. 2000. Relief effects for passive microwave remote sensing. *International Journal of Remote Sensing* 21: 2403–2412.

Mote, T. L., A. J. Grundstein, D. J. Leathers, and D. A. Robinson. 2003. A comparison of modeled, remotely sensed, and measured snow water equivalent in the northern Great Plains. *Water Resources Research* 39: 1209–1209.

Nagler, T., H. Rott, P. Malcher, and F. Muller. 2008. Assimilation of meteorological and remote sensing data for snowmelt runoff forecasting. *Remote Sensing of Environment* 112: 1408–1420.

Nash, J. E., and J. V. Sutcliffe. 1970. River flow forecasting through conceptual models part I—A discussion of principles. *Journal of Hydrology* 10: 282–290.

NCDC. 2010. *Climatology for Southwest Asia*. National Climatic Data Center.

Observatory, D. F. 2008. *Global archive of large flood events*. Dartmouth University.

Ohmura, A. 2001. Physical basis for the temperature-based melt-index method. *Journal of Applied Meteorology* 40: 753–761.

Parajka, J., and G. Bloschl. 2008. The value of MODIS snow cover data in validating and calibrating conceptual hydrologic models. *Journal of Hydrology* 358: 240–258.

Perkins, D. C., and J. K. Culbertson. 1970. *Hydrographic and sedimentation survey of Kajakai Reservoir, Afghanistan*. Geological Survey Water Supply Paper 1608-M, U.S. Geological Survey, Washington, D.C.

Rahman, S., A. C. Bagtzoglou, F. Hossain, L. Tang, L. D. Yarbrough, and G. Easson. 2009. Investigating spatial downscaling of satellite rainfall data for streamflow simulation in a medium-sized basin. *Journal of Hydrometeorology* 10: 1063–1079.

Rawlins, M. A., M. Fahnestock, S. Frolking, and C. J. Vorosmarty. 2007. On the evaluation of snow water equivalent estimates over the terrestrial Arctic drainage basin. *Hydrological Processes* 21: 1616–1623.

Sapiano, M. R. P., and P. A. Arkin. 2009. An intercomparison and validation of high-resolution satellite precipitation estimates with 3-hourly gauge data. *Journal of Hydrometeorology* 10: 149–166.

Stisen, S., and I. Sandholt. 2010. Evaluation of remote-sensing-based rainfall products through predictive capability in hydrological runoff modelling. *Hydrological Processes* 24: 879–891.

Tekeli, A.E. 2008 Early findings in comparison of AMRE-E/Aqua L3 global snow water equivalent EASE-grids data with in situ observations for Eastern Turkey. *Hydrological Processes* 22: 2737−2747.

UNESCO. 2009. *Third UN world water development report: Water in a changing world*. UN, Paris, France.

USACE. 1956. *Snow hydrology; summary of the snow investigations*. N. Pacific Division, COE, Portland, OR.

USACE. 1998. *Runoff from snowmelt*. Engineer Manual EM 1110-201406, U.S. Army Corps of Engineers.

USACE. 2007. *Water balance and regulation alternative analysis for Kajakai Reservoir using HEC-ResSim*. PR-63, U.S. Army Corps of Engineers.

USACE. 2009. *HEC-HMS hydrologic modeling system user's manual*. Hydrologic Engineering Center, Davis, CA.

USGS. 1979. *Daily streamflow data for Helmand River, Afghanistan*. USAID.

USGS. 2000. *Gap-filled SRTM digital elevation model of Afghanistan.* Reston, VA, U.S. Geological Survey.

USGS. 2007. *Water balance simulations of runoff and reservoir storage for the Upper Helmand Watershed and Kajakai Reservoir, Central Afghanistan.* Prepared for U.S. Agency for International Development.

Vining, K. C., and A. V. Vecchia. 2007. *Water-balance simulations of runoff and reservoir storage for the Upper Helmand Watershed and Kajakai Reservoir, Central Afghanistan.* Scientific Investigations Report 2007-5148 165, U.S. Geological Survey.

Walker, A., and B. Goodison. 1993. Discrimination of a wet snow cover using passive microwave satellite data. *Annals of Glaciology* 17: 307–311.

Williams-Sether, T. 2008. *Streamflow characteristics of streams in the Helmand Basin, Afghanistan*. Data Series 333, U.S. Geological Survey.

Wilson, L. L., L. Tsang, J. N. Hwang, and C. T. Chen. 1999. Mapping snow water equivalent by combining a spatially distributed snow hydrology model with passive microwave remote-sensing data. *IEEE Transactions on Geoscience and Remote Sensing* 37: 690–704.

Yang, D. Q., Y. Y. Zhao, R. Armstrong, and D. Robinson. 2009. Yukon River streamflow response to seasonal snow cover changes. *Hydrological Processes* 23: 109–121.

Yang, D. Q., Y. Y. Zhao, R. Armstrong, D. Robinson, and M. J. Brodzik. 2007. Streamflow response to seasonal snow cover mass changes over large Siberian watersheds. *Journal of Geophysical Research-Earth Surface* 112: S222–S222.

Appendix A: GIS Layers and Projection

Central Meridian:	67.0
Standard Parallel 1:	31.0
Standard Parallel 2:	37.0
Latitude of Origin:	23.0
Units:	Meters

Appendix B: SCA Error Matrices

2006–07 Winter

		SCA Imagery			
	25-Nov-06	Snow	No Snow		
HMS Snow	Snow	9290	6318	15608	users accuracy
Model	No Snow	4950	46484	51434	snow: 100.0%
		14240	52802	67042	no snow: 90.4%
					producers accuracy
		overall accuracy: 83.2%			snow: 65.2%
					no snow: 88.0%

8-Dec-06	Snow	No Snow		
Snow	24851	685	25536	users accuracy
No Snow	6208	14788	20996	snow: 97.3%
	31059	15473	46532	no snow: 70.4%
				producers accuracy
	overall accuracy: 85.2%			snow: 80.0%
				no snow: 95.6%

18-Dec-06	Snow	No Snow		
Snow	24348	4593	28941	users accuracy
No Snow	1299	16488	17787	snow: 84.1%
	25647	21081	46728	no snow: 92.7%
				producers accuracy
	overall accuracy: 87.4%			snow: 94.9%
				no snow: 78.2%

3-Jan-07	Snow	No Snow		
Snow	31701	5983	37684	users accuracy
No Snow	1215	7765	8980	snow: 84.1%
	32916	13748	46664	no snow: 86.5%
				producers accuracy
	overall accuracy: 84.6%			snow: 96.3%
				no snow: 56.5%

21-Jan-07	Snow	No Snow		
Snow	33476	10666	44142	users accuracy
No Snow	24	2443	2467	snow: 75.8%
	33500	13109	46609	no snow: 99.0%
				producers accuracy
	overall accuracy: 77.1%			snow: 99.9%
				no snow: 18.6%

16-Feb-07	Snow	No Snow		
Snow	25819	4198	30017	users accuracy
No Snow	119	10802	10921	snow: 86.0%
	25938	15000	40938	no snow: 98.9%
				producers accuracy
	overall accuracy: 89.5%			snow: 99.5%
				no snow: 72.0%

5-Mar-07	Snow	No Snow			
Snow	28848	3848	32696	users accuracy	
No Snow	112	13905	14017	snow:	88.2%
	28960	17753	46713	no snow:	99.2%
				producers accuracy	
	overall accuracy:	91.5%		snow:	99.6%
				no snow:	78.3%

14-Mar-07	Snow	No Snow			
Snow	27129	3614	30743	users accuracy	
No Snow	250	14577	14827	snow:	88.2%
	27379	18191	45570	no snow:	98.3%
				producers accuracy	
	overall accuracy:	91.5%		snow:	99.1%
				no snow:	80.1%

27-Mar-07	Snow	No Snow			
Snow	19166	7130	26296	users accuracy	
No Snow	546	19707	20253	snow:	72.9%
	19712	26837	46549	no snow:	97.3%
				producers accuracy	
	overall accuracy:	83.5%		snow:	97.2%
				no snow:	73.4%

1-May-07	Snow	No Snow			
Snow	171	115	286	users accuracy	
No Snow	1056	44658	45714	snow:	59.8%
	1227	44773	46000	no snow:	97.7%
				producers accuracy	
	overall accuracy:	97.5%		snow:	13.9%
				no snow:	99.7%

14-May-07	Snow	No Snow			
Snow	18	2	20	users accuracy	
No Snow	181	46484	46665	snow:	100.0%
	199	46486	46685	no snow:	99.6%
				producers accuracy	
	overall accuracy:	99.6%		snow:	9.0%
				no snow:	100.0%

2007–08 Winter

25-Nov-07	Snow	No Snow	
Snow	0	1501	1501
No Snow	0	45227	45227
	0	46728	46728

overall accuracy: 96.8%

users accuracy
snow: 0.0%
no snow: 100.0%
producers accuracy
snow: 100.0%
no snow: 96.8%

8-Dec-07	Snow	No Snow	
Snow	5476	3910	9386
No Snow	10	4014	4024
	5486	7924	13410

overall accuracy: 70.8%

users accuracy
snow: 58.3%
no snow: 99.8%
producers accuracy
snow: 99.8%
no snow: 50.7%

16-Dec-07	Snow	No Snow	
Snow	19232	8791	28023
No Snow	992	17713	18705
	20224	26504	46728

overall accuracy: 79.1%

users accuracy
snow: 68.6%
no snow: 94.7%
producers accuracy
snow: 95.1%
no snow: 66.8%

25-Dec-07	Snow	No Snow	
Snow	26781	3956	30737
No Snow	530	15342	15872
	27311	19298	46609

overall accuracy: 90.4%

users accuracy
snow: 87.1%
no snow: 96.7%
producers accuracy
snow: 98.1%
no snow: 79.5%

31-Dec-07	Snow	No Snow	
Snow	24131	9886	34017
No Snow	306	12405	12711
	24437	22291	46728

overall accuracy: 78.2%

users accuracy
snow: 70.9%
no snow: 97.6%
producers accuracy
snow: 98.7%
no snow: 55.7%

21-Jan-08	Snow	No Snow	
Snow	37832	6647	44479
No Snow	304	1945	2249
	38136	8592	46728

overall accuracy: 85.1%

users accuracy
snow: 85.1%
no snow: 86.5%
producers accuracy
snow: 99.2%
no snow: 22.6%

7-Feb-08	Snow	No Snow	
Snow	42545	3956	46501
No Snow	64	163	227
	42609	4119	46728

overall accuracy: 91.4%

users accuracy
snow: 91.5%
no snow: 71.8%
producers accuracy
snow: 99.8%
no snow: 4.0%

19-Feb-08	Snow	No Snow		
Snow	35763	6674	42437	users accuracy
No Snow	23	4268	4291	snow: 84.3%
	35786	10942	46728	no snow: 99.5%
				producers accuracy
	overall accuracy: 85.7%			snow: 99.9%
				no snow: 39.0%

1-Mar-08	Snow	No Snow		
Snow	23579	13077	36656	users accuracy
No Snow	1	10071	10072	snow: 64.3%
	23580	23148	46728	no snow: 100.0%
				producers accuracy
	overall accuracy: 72.0%			snow: 100.0%
				no snow: 43.5%

16-Mar-08	Snow	No Snow		
Snow	10053	8262	18315	users accuracy
No Snow	1313	27100	28413	snow: 54.9%
	11366	35362	46728	no snow: 95.4%
				producers accuracy
	overall accuracy: 79.5%			snow: 88.4%
				no snow: 76.6%

31-Mar-08	Snow	No Snow		
Snow	1749	2110	3859	users accuracy
No Snow	754	42115	42869	snow: 45.3%
	2503	44225	46728	no snow: 98.2%
				producers accuracy
	overall accuracy: 93.9%			snow: 69.9%
				no snow: 95.2%

12-Apr-08	Snow	No Snow		
Snow	2224	128	2352	users accuracy
No Snow	2145	42231	44376	snow: 94.6%
	4369	42359	46728	no snow: 95.2%
				producers accuracy
	overall accuracy: 95.1%			snow: 50.9%
				no snow: 99.7%

16-Apr-08	Snow	No Snow		
Snow	2236	10	2246	users accuracy
No Snow	10681	33801	44482	snow: 99.6%
	12917	33811	46728	no snow: 76.0%
				producers accuracy
	overall accuracy: 77.1%			snow: 17.3%
				no snow: 100.0%

29-Apr-08	Snow	No Snow		
Snow	589	87	676	users accuracy
No Snow	633	45258	45891	snow: 87.1%
	1222	45345	46567	no snow: 98.6%
				producers accuracy
	overall accuracy: 98.5%			snow: 48.2%
				no snow: 99.8%

12-May-08	Snow	No Snow		
Snow	163	30	193	users accuracy
No Snow	192	46098	46290	snow: 84.5%
	355	46128	46483	no snow: 99.6%
				producers accuracy
	overall accuracy: 99.5%			snow: 45.9%
				no snow: 99.9%

2008-09 Winter

5-Nov-08	Snow	No Snow		
Snow	437	1388	1825	users accuracy
No Snow	30	44858	44888	snow: 23.9%
	467	46246	46713	no snow: 99.9%
				producers accuracy
	overall accuracy: 97.0%			snow: 93.6%
				no snow: 97.0%

23-Nov-08	Snow	No Snow		
Snow	1147	16762	17909	users accuracy
No Snow	50	28769	28819	snow: 6.4%
	1197	45531	46728	no snow: 99.8%
				producers accuracy
	overall accuracy: 64.0%			snow: 95.8%
				no snow: 63.2%

10-Dec-08	Snow	No Snow		
Snow	10999	1353	12352	users accuracy
No Snow	11224	22844	34068	snow: 89.0%
	22223	24197	46420	no snow: 67.1%
				producers accuracy
	overall accuracy: 72.9%			snow: 49.5%
				no snow: 94.4%

22-Dec-08	Snow	No Snow		
Snow	27882	1617	29499	users accuracy
No Snow	5577	10870	16447	snow: 94.5%
	33459	12487	45946	no snow: 66.1%
				producers accuracy
	overall accuracy: 84.3%			snow: 83.3%
				no snow: 87.1%

8-Jan-09	Snow	No Snow		
Snow	26656	3162	29818	users accuracy
No Snow	3368	13542	16910	snow: 89.4%
	30024	16704	46728	no snow: 80.1%
				producers accuracy
	overall accuracy: 86.0%			snow: 88.8%
				no snow: 81.1%

23-Jan-09	Snow	No Snow		
Snow	29989	2665	32654	users accuracy
No Snow	458	5633	6091	snow: 91.8%
	30447	8298	38745	no snow: 92.5%
				producers accuracy
	overall accuracy: 91.9%			snow: 98.5%
				no snow: 67.9%

8-Feb-09	Snow	No Snow		
Snow	32711	1611	34322	users accuracy
No Snow	1109	11297	12406	snow: 95.3%
	33820	12908	46728	no snow: 91.1%
				producers accuracy
	overall accuracy: 94.2%			snow: 96.7%
				no snow: 87.5%

7-Mar-09	Snow	No Snow		
Snow	21438	5194	26632	users accuracy
No Snow	499	18402	18901	snow: 80.5%
	21937	23596	45533	no snow: 97.4%
				producers accuracy
	overall accuracy: 87.5%			snow: 97.7%
				no snow: 78.0%

14-Mar-09	Snow	No Snow		
Snow	19328	4192	23520	users accuracy
No Snow	1261	21947	23208	snow: 82.2%
	20589	26139	46728	no snow: 94.6%
				producers accuracy
	overall accuracy: 88.3%			snow: 93.9%
				no snow: 84.0%

25-Mar-09	Snow	No Snow		
Snow	11661	1562	13223	users accuracy
No Snow	8248	25257	33505	snow: 88.2%
	19909	26819	46728	no snow: 75.4%
				producers accuracy
	overall accuracy: 79.0%			snow: 58.6%
				no snow: 94.2%

30-Mar-09	Snow	No Snow		
Snow	7785	1676	9461	users accuracy
No Snow	5257	24242	29499	snow: 82.3%
	13042	25918	38960	no snow: 82.2%
				producers accuracy
	overall accuracy: 82.2%			snow: 59.7%
				no snow: 93.5%

17-Apr-09	Snow	No Snow			
Snow	4567	747	5314	users accuracy	
No Snow	5458	34700	40158	snow:	85.9%
	10025	35447	45472	no snow:	86.4%
				producers accuracy	
	overall accuracy: 86.4%			snow:	45.6%
				no snow:	97.9%

5-May-09	Snow	No Snow			
Snow	1486	340	1826	users accuracy	
No Snow	3042	41841	44883	snow:	81.4%
	4528	42181	46709	no snow:	93.2%
				producers accuracy	
	overall accuracy: 92.8%			snow:	32.8%
				no snow:	99.2%

18-May-09	Snow	No Snow			
Snow	290	14	304	users accuracy	
No Snow	1752	44664	46416	snow:	95.4%
	2042	44678	46720	no snow:	96.2%
				producers accuracy	
	overall accuracy: 96.2%			snow:	14.2%
				no snow:	100.0%

Appendix C: SWE Spatial Analysis

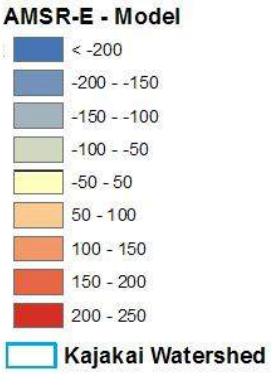

Legend.

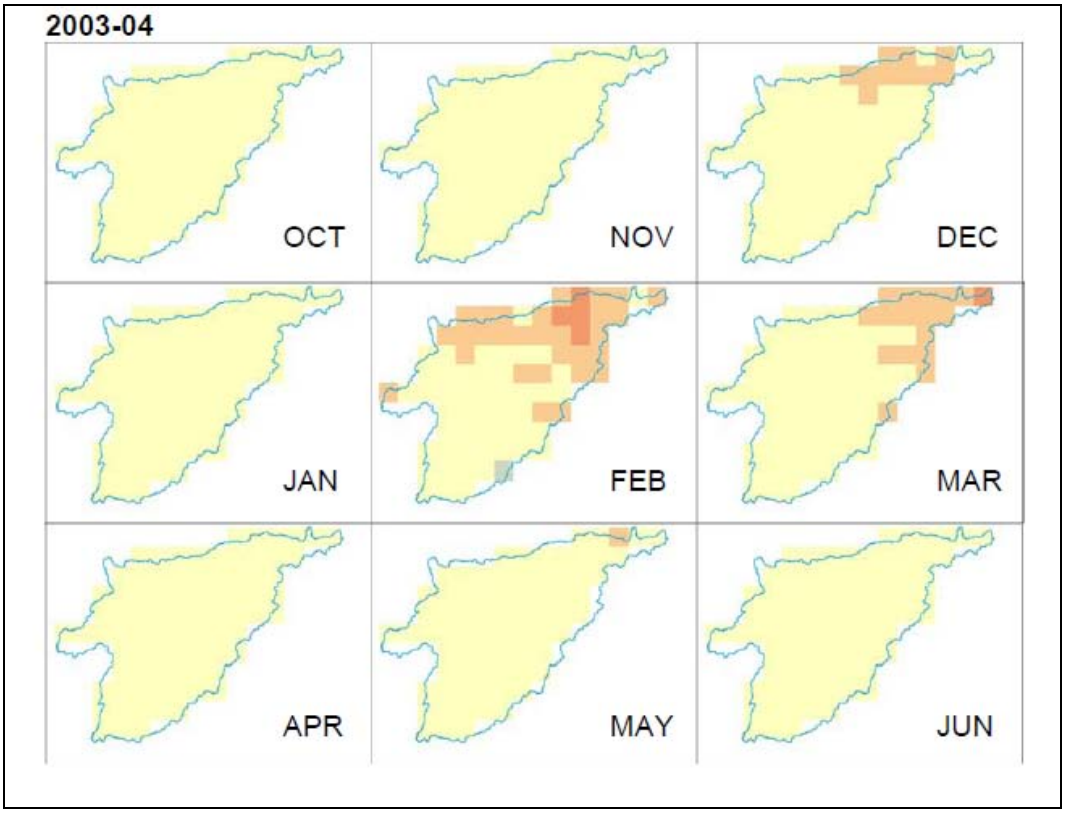

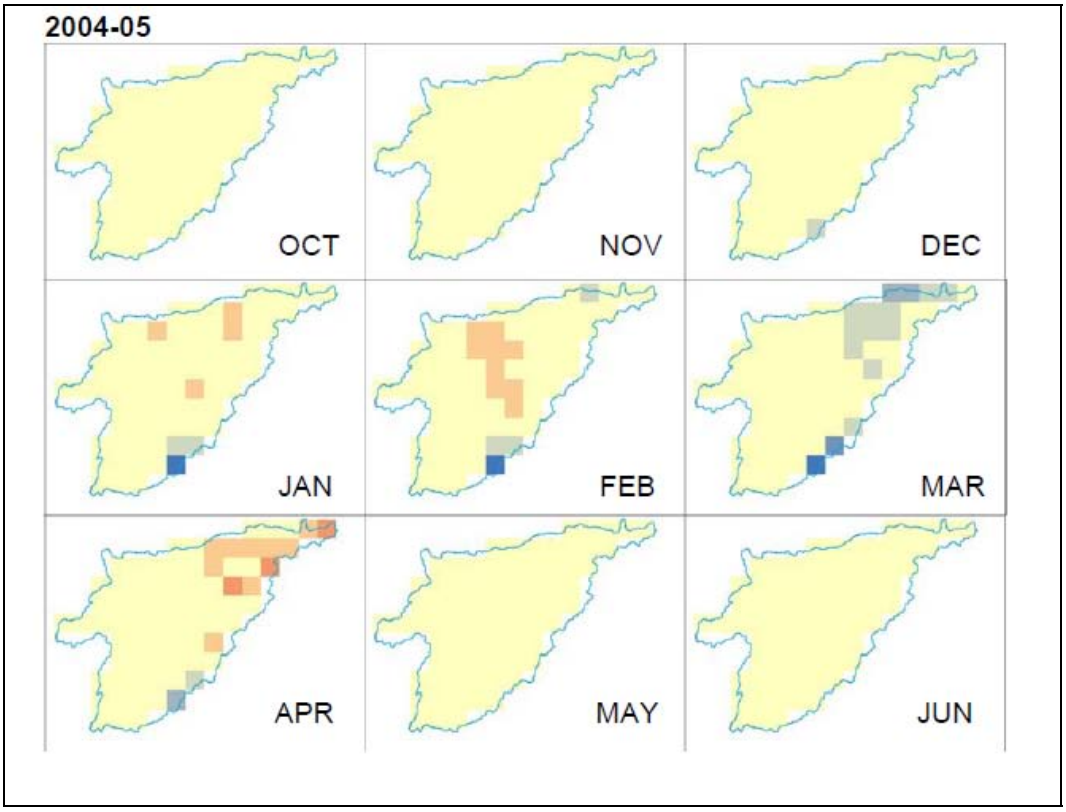
2004-05
OCT
NOV
DEC
JAN
FEB
MAR
APR
MAY
JUN

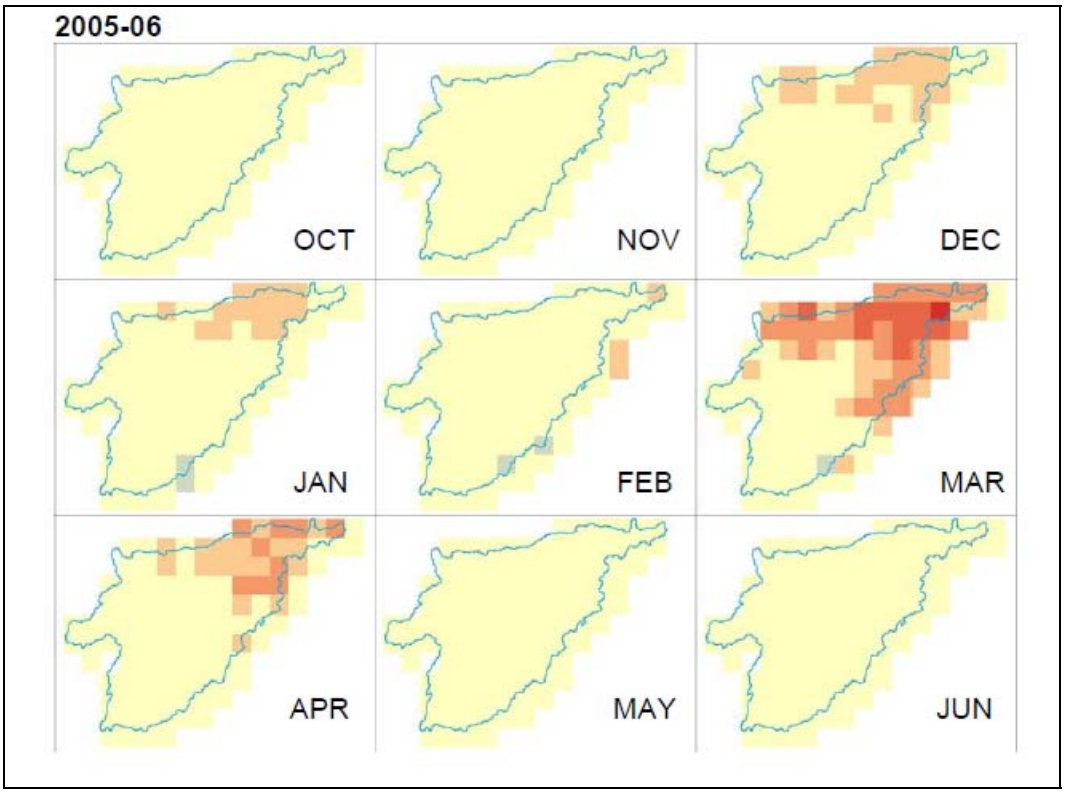
2005-06
OCT
NOV
DEC
JAN
FEB
MAR
APR
MAY
JUN

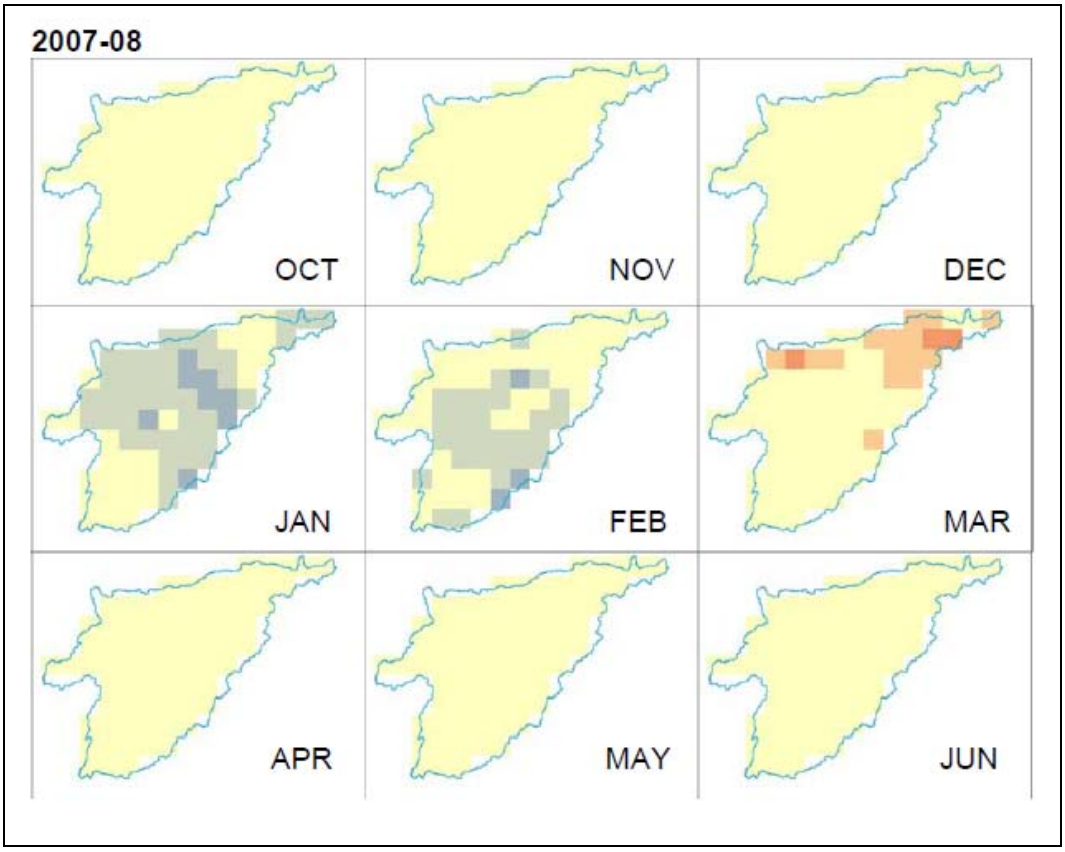
2007-08
OCT
NOV
DEC
JAN
FEB
MAR
APR
MAY
JUN

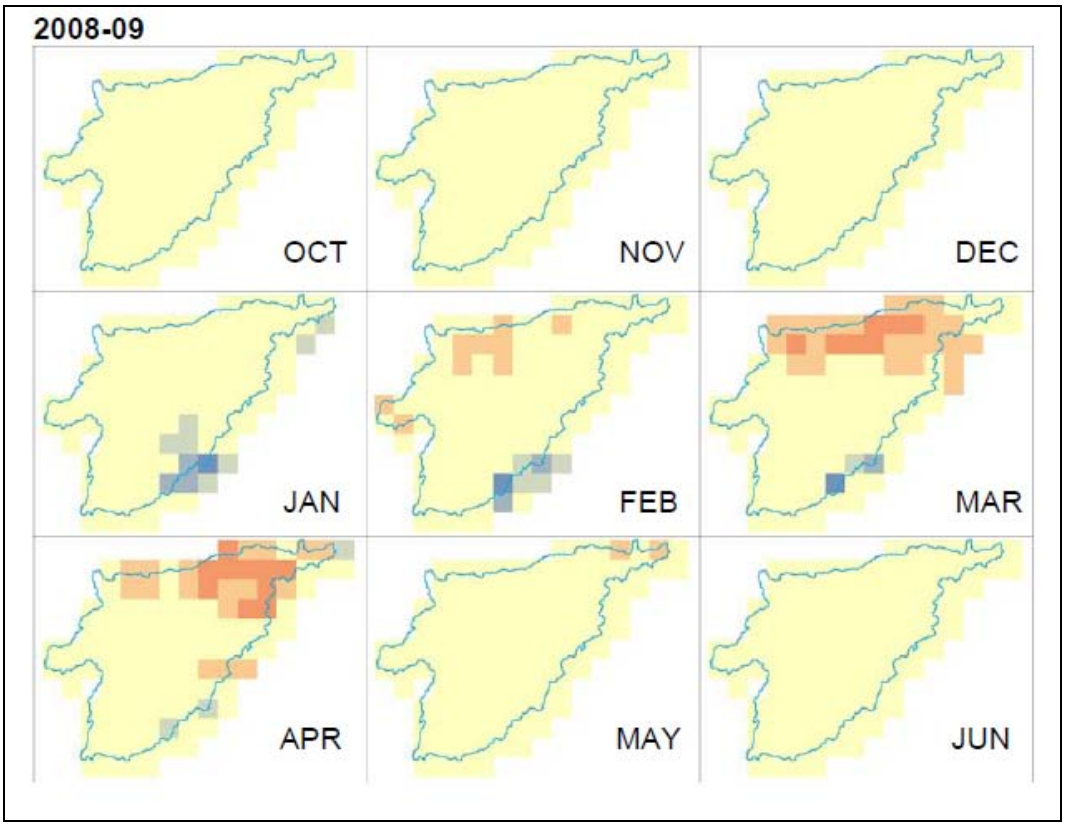
2008-09
OCT
NOV
DEC
JAN
FEB
MAR
APR
MAY
JUN

REPORT DOCUMENTATION PAGE

Form Approved
OMB No. 0704-0188

1. REPORT DATE *(DD-MM-YYYY)*	2. REPORT TYPE	3. DATES COVERED *(From - To)*
March 2011		

4. TITLE AND SUBTITLE

Assessing the Accuracy of Passive Microwave Estimates of Snow Water Equivalent in Data-Scarce Regions for Use in Water Resource Applications:

A case study in the Upper Helmand Watershed, Afghanistan

5a. CONTRACT NUMBER

5b. GRANT NUMBER

5c. PROGRAM ELEMENT NUMBER

6. AUTHOR(S)

Carrie M. Vuyovich

5d. PROJECT NUMBER

5e. TASK NUMBER

5f. WORK UNIT NUMBER

7. PERFORMING ORGANIZATION NAME(S) AND ADDRESS(ES)

Cold Regions Research and Engineering Laboratory
U.S. Army Engineer Research and Development Center
72 Lyme Road
Hanover, NH 03755

8. PERFORMING ORGANIZATION REPORT NUMBER

ERDC-CRREL TR-11-8

9. SPONSORING / MONITORING AGENCY NAME(S) AND ADDRESS(ES)

HQ-USACE
Washington DC

10. SPONSOR/MONITOR'S ACRONYM(S)

11. SPONSOR/MONITOR'S REPORT NUMBER(S)

12. DISTRIBUTION / AVAILABILITY STATEMENT

Approved for public release; distribution is unlimited.

13. SUPPLEMENTARY NOTES

14. ABSTRACT

Winter snowpack is a significant contributor to water supply in many regions of the world and accurate estimates of the snow water equivalent (SWE) are necessary for water resource planning. Satellite data are an attractive source of snow information in remote regions with limited ground data. The objective of this study is to assess passive microwave SWE in the Upper Helmand Watershed in Afghanistan where snowmelt is a primary source of water. Passive microwave SWE data were compared over six winter seasons, 2004–2009, to an independent estimate of SWE using a snow hydrology model. The snow hydrology model was calibrated to high-resolution snow covered area images and observed reservoir levels. The model was initialized with passive microwave SWE data and found to improve results in years when input precipitation was low. The results showed that passive microwave SWE has potential to provide valuable water resource information in this data-scarce region.

15. SUBJECT TERMS

Afghanistan
Passive microwave SWE data
Satellite data
Snow hydrology model
Snow water equivalent (SWE)
Upper Helmand Watershed

16. SECURITY CLASSIFICATION OF:			17. LIMITATION OF ABSTRACT	18. NUMBER OF PAGES	19a. NAME OF RESPONSIBLE PERSON
a. REPORT	b. ABSTRACT	c. THIS PAGE			19b. TELEPHONE NUMBER *(include area code)*
U	U	U	none	84	